Economic Geology, v. 119, no. 8, pp. 1833–1859

Mineralogy and Paragenesis of the Boundary Zone Zn-Pb ± Ag Deposit, Yukon, Canada

Haruna M. Grema,[1,2,†] Joseph M. Magnall,[1] Sarah A. Gleeson,[1,2] Jack E. Milton,[3] Alicja Wudarska,[1,4] Anja M. Schleicher,[1] and Hans-Martin Schulz[1]

[1] *GFZ German Research Centre for Geosciences, Telegrafenberg, 14473 Potsdam, Germany*

[2] *Institute of Geological Sciences, Freie Universität Berlin, Malteserstrasse 74-100, 12249 Berlin, Germany*

[3] *Fireweed Metals Corporation, Suite 2800, Four Bentall Centre, 1055 Dunsmuir Street, Vancouver V7X 1L2, British Columbia, Canada*

[4] *Institute of Geological Sciences, Polish Academy of Sciences, Twarda 51/55, 00-818 Warsaw, Poland*

Abstract

Clastic-dominated (CD-type) Zn-Pb ± Ag deposits account for significant global Zn and Pb resources. In this contribution, we describe a new Zn-Pb ± Ag deposit, Boundary Zone, recently discovered in the Macmillan Pass district, Yukon, Canada. Nine drill holes were sampled and studied using petrography, mineralogy (whole-rock and clay fraction X-ray diffractometry), and U-Pb geochronology on fluorapatite. These methods were used to develop a mineralogical paragenesis in order to constrain the timing of and controls on sulfide mineralization.

The mineralization at Boundary Zone is hosted by the Late Ordovician-Early Silurian Duo Lake and the Middle-Late Devonian Portrait Lake Formations. The discovery of mineralized Ordovician-Silurian rocks at Boundary Zone is the first time that significant stratabound mineralization has been identified in rocks of this age within the Macmillan Pass district. The premineralization stage is dominated by early diagenetic phases, including quartz, barite, pyrite, fluorapatite, and phyllosilicates. Two genetically distinct mineralization stages have been identified. Mineralization stage I comprises stratabound fine-grained sphalerite, pyrite, galena, sulfosalts, and barian mica. Mineralization stage I sulfides formed via barite replacement, nucleation on premineralization pyrite, and porosity exploitation during early biogenic silica transformation of opal-A to cryptocrystalline and microquartz in highly siliceous mudstones (up to 85 wt % quartz). The high-grade and volumetrically major mineralization stage II formed following significant hydrothermal fluid-induced brecciation and veining of the host rocks and is accompanied by silicification and siderite formation. The presence of kaolinite, pyrophyllite, quartz, and fluorapatite suggests that hydrothermal fluids were likely F rich with temperatures up to 240°C.

In one sample from the Niddery Lake Member, a discordant vein crosscuts mineralization stage I, but its paragenetic relationship with mineralization stage II could not be determined. Fluorapatite in this vein records a Middle Jurassic U-Pb age. We suggest the multiple mineralizing events at Boundary Zone formed during a prolonged period of fluid flow, spanning from diagenetic stages in the basin, possibly to periods of Cordilleran-related deformation in the Selwyn basin. These findings have significant implications for exploration strategies in the Macmillan Pass district and similar geologic settings, where biosiliceous mudstone deposition, diagenetic barite formation, and multiple hydrothermal fluid pulses are evident.

Introduction

Clastic-dominated (CD-type) deposits are stratiform and stratabound massive sulfide deposits commonly hosted in fine-grained siliciclastic-carbonate rocks (Leach et al., 2005). These deposits contain some of the largest Zn and Pb resources and associated critical metals (e.g., Ge, Ga, In), and an increasing demand relating to the green transition has driven a new wave of exploration for these resources (Jowitt and McNulty, 2021; Valckx et al., 2021). A small number of ancient sedimentary basins (North Australian Proterozoic and North American Paleozoic margins) contain the largest CD-type deposits, and the most notable recent discoveries have been made during brownfield exploration programs in well-endowed, world-class provinces (e.g., Teena deposit, Carpentaria Province; Hayward et al., 2021).

The Selwyn basin (Canada; Fig. 1A) is one of the top three CD-type provinces in the world (Goodfellow and Lydon, 2007). Mineralized rocks are hosted across three broad stratigraphic intervals within Paleozoic units (Fig. 1B), which are all characterized by periods of carbonaceous mudstone deposition (Abbott and Turner, 1991). Major Selwyn basin deposits are located in (1) the Anvil district, where sulfide mineralized rocks are hosted by Cambrian units that have been highly deformed and subjected to greenschist facies metamorphism (Jennings and Jilson, 1986; Pigage, 1991); (2) the Howard's Pass district, where sulfide mineralized rocks are hosted by Late Ordovician to Early Silurian units (Morganti, 1979); and (3) the Macmillan Pass district, where sulfide mineralized rocks are well preserved in Middle to Late Devonian units (Turner, 1986; Goodfellow and Lydon, 2007; Magnall et al., 2016b). Both the Howard's Pass and Macmillan Pass districts have been metamorphosed to subgreenschist facies grade with varying degrees of tectonic overprint (McClay, 1984; Gordey and Anderson, 1993; Martel, 2017).

In the Macmillan Pass district (Fig. 1C), genetic models have been developed at two localities (Tom and Jason) where

†Corresponding author: e-mail, hgrema@gfz-potsdam.de

 Submitted: March 4, 2024 / Accepted: September 2, 2024

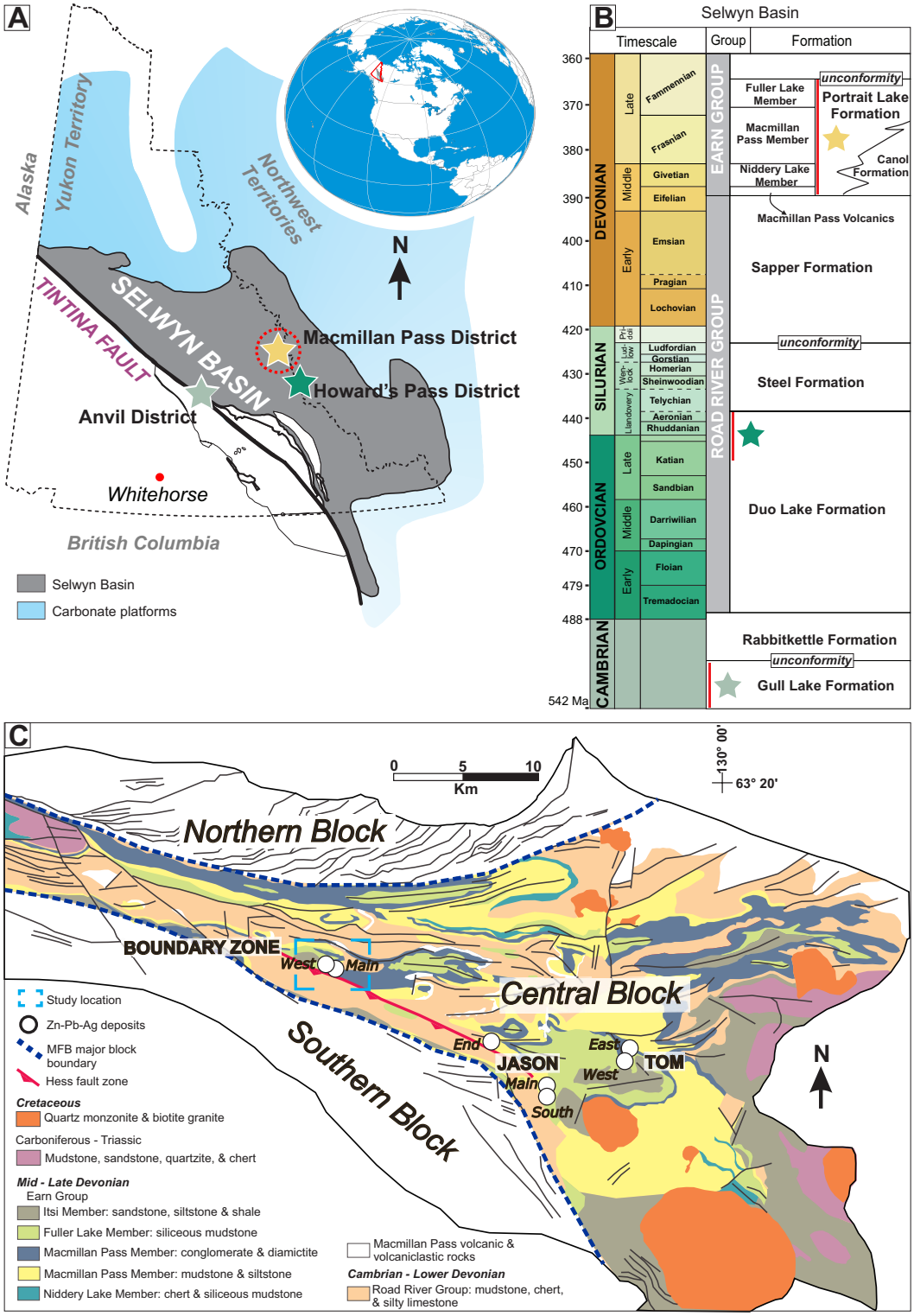

Fig. 1. General overview of the geology and stratigraphy of the Selwyn basin with details of the Macmillan Pass area. (A) Location and simplified geologic map of the Selwyn basin in the Yukon Territory, Canada. The three major Zn districts of the basin are denoted by stars, with that of the Macmillan Pass district highlighted in a red circle. Modified from Goodfellow (2007). (B) Stratigraphy of the Selwyn basin from the Cambrian to Devonian periods. The Portrait Lake Formation is further subdivided into individual members. Volcaniclastic rocks occur at the bottom of the Portrait Lake Formation and are interbedded with the Macmillan Pass Member. The Macmillan Pass Member comprises the mudstone, conglomerate, and diamictite units. Modified from Nelson and Colpron (2007). (C) Geologic map of the Macmillan fold belt (MFB) region, highlighting the facies in the Central block. The locations of the Tom and Jason deposits and the Boundary Zone deposit are shown. Modified from Turner and Rhodes (1990) and Abbott (2013).

the complete deposit architecture is well preserved (Fig. 2). Early studies on the Tom and Jason deposits led to the development of the sedimentary exhalative (SEDEX) model (Carne and Cathro, 1982; Goodfellow, 1987; Goodfellow et al., 1993), which has since been more broadly applied to CD-type deposits in other districts (e.g., Rajabi et al., 2015). In this model (Fig. 2A), mineralization-stage sulfides formed following fault-bound exhalation of hydrothermal Zn-Pb ± Ba-rich fluids into an H_2S-bearing (euxinic) water column (Goodfellow, 2007). In many deposits, there is no direct evidence of a fault-bound feeder zone preserved in the rock record (e.g., Howards Pass district); therefore, the exhalation of dense, bottom-hugging brines (Fig. 2B) has been invoked as a mechanism for sulfide precipitation in topographic depressions on the sea floor, away from sites of venting (Sangster, 2002). However, studies in the Selwyn and McArthur basins have suggested that sulfide mineralization formed during the early to burial stages of diagenesis via host-rock replacement (Williams, 1978a, b; Morganti, 1981; Gadd et al., 2017; Magnall et al., 2020). At Macmillan Pass, Magnall et al. (2020) proposed a two-stage model involving diagenetic preenrichment of the host rock in sulfur, in the form of barite and pyrite (Fig. 2C), which was then replaced by mineralization-stage sulfides (Fig. 2D).

The recent discovery at Boundary Zone (Macmillan Pass district) provides an excellent example of successful exploration within a long-known district. The Boundary Zone deposit comprises sulfide-mineralized rocks that are located west of the Tom and Jason deposits (Fig. 1C). The Boundary Zone deposit is situated in an area historically known as Boundary Creek (Abbott and Turner, 1991), where stockwork-vein-style mineralization was drilled in the 1980s and was interpreted as being a feeder zone of a SEDEX deposit (Turner and Rhodes, 1990). Recent drilling programs by Fireweed Metals Corporation have discovered extensive mineralization at Boundary Zone in two different stratigraphic units: the Late Ordovician to Early Silurian Duo Lake Formation (part of the Road River Group, which hosts the Howard's Pass district mineralization; Morganti, 1979) and the Middle to Late Devonian Portrait Lake Formation (Earn Group), also host to the Tom and Jason deposits (Gardner and Hutcheon, 1985; Bailes et al., 1986). The presence of multiple mineralized zones in differ-

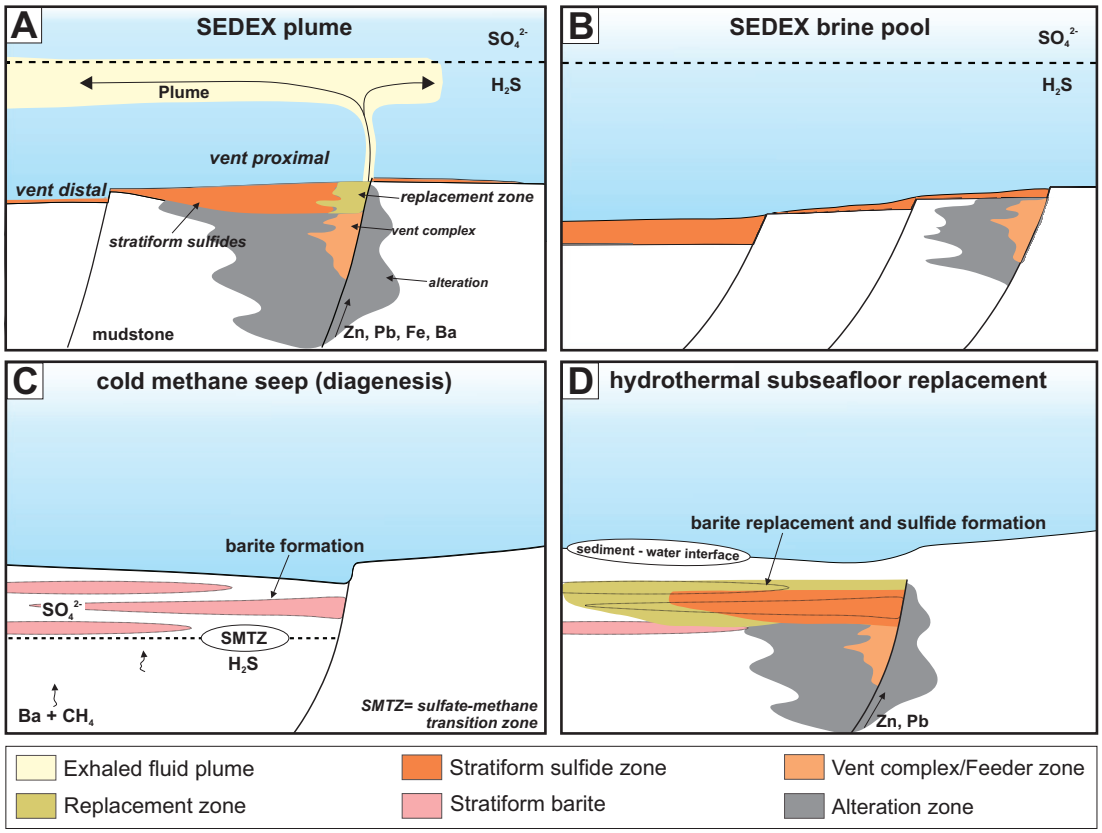

Fig. 2. Schematic diagrams of the genetic models suggested for the formation of Zn-Pb ± Ba deposits in the Selwyn basin. (A) The sedimentary exhalative (SEDEX) model comprises a stratified water column where metalliferous hydrothermal fluids are exhaled. Sulfide minerals precipitate in the reduced sulfur (H_2S-rich), anoxic to euxinic bottom water. Barite forms in the sulfate (SO_4^{2-})-saturated zone of the water column and may be found with both the proximal and distal sulfide assemblages, modified from Goodfellow et al. (1993). (B) The brine pool model is a modified version of the SEDEX model in which hydrothermal fluids are exhaled into the water column and migrate, as part of bottom water-hugging dense brines, to depressions on the sea floor where sulfides form, modified from Sangster (2002). (C-D) Two-stage genetic model for the formation of Zn-Pb ± Ba deposits. In the cold methane seep model, fluids rich in barium (Ba) and methane (CH_4) are delivered into a sulfate-saturated sediment column, resulting in diagenetic precipitation of barite (C). Adapted from Torres et al. (2003). Hydrothermal fluids infiltrating the shallow subseafloor result in the dissolution of barite and the subsequent precipitation of sulfide minerals through subsurface diagenetic replacement (D). Modified from Magnall et al. (2020).

ent stratigraphic intervals is unique among CD-type deposits in the Selwyn basin and could provide new perspectives on sulfide mineralization in the basin and CD-type deposits more broadly.

In this study, samples obtained from nine drill holes intersecting the Boundary Zone deposit have been investigated. This study has utilized (1) a combination of petrographic techniques, including rreflected- and transmitted-light microscopy, cathodoluminescence (CL) imaging, electron probe microanalysis (EPMA), and scanning electron microscopy (SEM); (2) quantitative X-ray diffractometry (QXRD) of bulk rock powders and semiquantitative analyses of clay-size fraction; and (3) fluorapatite U-Pb dating with secondary ion mass spectrometry (SIMS). The primary objectives of this study were to characterize the mineralogy of the host rocks and diagenetic assemblages and determine the timing of the sulfide mineralization and associated alteration assemblages. The results provide the first mineralogical and paragenetic description of Boundary Zone, which indicates a multistage hydrothermal system that spanned host-rock diagenesis through to Cordilleran-stage deformation in the Selwyn basin.

Background Geology

Selwyn basin

The Selwyn basin is bounded by the Mackenzie carbonate platform to the east and by accreted terranes and the Tintina fault to the west (Fig. 1A; Gabrielse, 1967). The formation of the basin followed protracted extensional tectonics and the breakup of the Rodinian supercontinent, which led to the reemergence of the Laurentian craton between 775 and 720 Ma (Milton et al., 2017). A 4- to 6-km-thick sequence of Neoproterozoic-Terreneuvian synrift strata comprises the Windermere Supergroup, which represents the oldest stratigraphic unit in the Selwyn basin (Gordey and Anderson, 1993). During the Paleozoic, a thick sequence of postrift clastic sedimentary rocks was deposited over the basal strata as the depositional environment evolved into deeper water conditions (Gordey and Anderson, 1993).

The basal part of the Paleozoic sequence comprises the Early to Middle Cambrian Gull Lake Formation (Fig. 1B), which is overlain by the Late Cambrian to Early Ordovician limestones and siltstones of the Rabbitkettle Formation (Gordey and Anderson, 1993). The Road River Group overlies the Rabbitkettle Formation and comprises Early Ordovician to Early Devonian strata. The overlying deep marine Middle to Late Devonian Earn Group consists of an abrupt change in facies development characterized by variable lithological thickness and unconformities (Abbott et al., 1986; Mair et al., 2006).

Three phases of alkalic to ultrapotassic volcanic activity occurred during the Early Cambrian, Early to Middle Ordovician, and Middle to Late Devonian (Goodfellow, 1987; Abbott and Turner, 1991; Cobbett et al., 2020). The volcanism has been interpreted to represent intermittent rifting and extension of the continental margin (Gordey and Anderson, 1993), concomitant with the melting of the heterogeneous lithospheric mantle (e.g., Goodfellow et al., 1995; Scanlan, 2022).

In the Jurassic, island arc accretion resulted in the Selwyn basin strata being incorporated into the fold-and-thrust belt of the North American Cordillera (Monger et al., 1982; Nelson and Colpron, 2007). Regional deformation resulted in open to tight folds, axial planar slaty cleavage, and gently dipping thrust faults (Gordey et al., 2010; Martel, 2017). The Cordilleran deformation terminated during the Late Cretaceous (~100 Ma) and was followed by postorogenic plutonism and emplacement of intermediate to felsic granitoids with ages of ~110 to 90 Ma (Gordey and Anderson, 1993; Hart et al., 2004; Gordey et al., 2010).

The Selwyn basin hosts three major Zn-Pb mineralized districts. In the Anvil district, five deposits had a combined premining mineral resource of 120 Mt at 5.6% Zn, 3.7% Pb, and 45 to 50 g/t Ag (Jennings and Jilson, 1986) and are hosted in phyllites and schists of the Mount Mye Formation, which is time equivalent to the Gull Lake Formation (Pigage, 1991). The Howard's Pass district consists of fourteen deposits hosted in the Late Ordovician to Early Silurian Duo Lake Formation of the Road River Group (Morganti, 1979; Slack et al., 2017), with a combined estimated 400.7 Mt grading at 4.5% Zn and 1.5% Pb (Kirkham et al., 2012). Sulfide mineralization mainly occurs in carbonaceous, siliceous, and calcareous mudstones and cherts of the Active Member, with gangue mineral phases such as pyrite, quartz, calcite, and apatite (Jonasson et al., 1986; Gadd et al., 2017). The overlying siliceous mudstones of the informal Upper Siliceous Mudstone and Backside Siliceous Mudstone (Portrait Lake Formation) Members in the Howard's Pass district have also been shown to host minor sulfide mineralization (Gadd et al., 2016b; Slack et al., 2017). The Zn-Pb ± Ba mineralization in the Macmillan Pass district is hosted mainly in carbonaceous and biosiliceous mudstones of the Middle to Late Devonian Portrait Lake Formation (Goodfellow, 2004; Magnall et al., 2015). The Tom, Jason, End Zone, and Boundary Zone deposits in the Macmillan Pass district currently have a combined indicated resource of 56.0 Mt at 5.49% Zn, 1.58% Pb, and 24.2 g/t Ag, with inferred resources of 48.5 Mt at 5.15% Zn, 2.08% Pb, and 25.3 g/t Ag (Landry et al., 2024). In the following section, the key features of the Macmillan Pass district are discussed in further detail.

Stratigraphy of the Macmillan Pass district

The Macmillan Pass district is located at the eastern margin of the Selwyn basin, at the border between the Northwest Territories and Yukon (Fig. 1A). The district is within the Macmillan fold belt, which formed as a result of Mesozoic accretionary deformation and comprises west-trending tight folds that deformed the Paleozoic sequences of the Earn Group and sulfide mineralization (Abbott and Turner, 1991). Based on field mapping, Abbott (1982) defined three tectonostratigraphic domains in the Macmillan fold belt: the Northern, Central, and Southern blocks that encompass the Macmillan Pass district (Fig. 1C). The Macmillan Pass district is located in the Central Block, which is distinguished from surrounding blocks by the presence of volcanic rocks, diamictites, and certain stratigraphic units that are absent elsewhere, implying the presence of syndepositional faults (Turner and Rhodes, 1990; Abbott and Turner, 1991). Stratiform barite deposits occur in both the Northern and Southern blocks of the Macmillan fold belt, including the Walt barite deposit in the Northern block (Abbott and Turner, 1991).

Road River Group: The Road River Group comprises Early Ordovician to Late Silurian mudstone, chert, and limestone units overlying deep-water carbonates and shales of the Gull Lake Formation (Abbott and Turner, 1991; Abbott, 2013). The group is divided into the Duo Lake, Steel, and Sapper Formations (Fig. 1B). Graptolite biostratigraphy constrains the age of the Duo Lake Formation to the Late Tremadocian (~479 Ma, Lower Ordovician) to Early Wenlock (~423 Ma, Silurian; Cecile, 1982). It comprises bedded siliceous mudstones and cherts that are overlain by a package of black siliceous mudstones and cherts (Abbott, 2013). Conformably overlying the Duo Lake Formation is the Steel Formation, comprising dark gray, wispy laminated and bioturbated mudstone (Gordey and Anderson, 1993). The Road River Group's youngest strata comprise the Sapper Formation, consisting of recessive silty limestone and calcareous black mudstone (Abbott, 2013) and constrained to the Late Eifelian age (~390 Ma; Fraser et al., 2021).

Earn Group: The Earn Group overlies the Road River Group and is divided into the Portrait Lake and Itsi Formations (Abbott et al., 1986; Abbott, 2013). The age of the Portrait Lake Formation ranges from Givetian to Famennian (387–358 Ma), constrained by conodont biostratigraphy (Abbott, 2013), and is host to the Tom and Jason deposits at Macmillan Pass.

The Macmillan Pass area hosts the type section of the Portrait Lake Formation (Cecile, 2000; Martel et al., 2011), which is broadly time equivalent to the Canol Formation in the Mackenzie Mountains (Blusson, 1978; Carne, 1979; Abbott and Turner, 1991). The Portrait Lake Formation comprises the informal Niddery Lake, Macmillan Pass, and Fuller Lake Members, which are underlain by and interbedded with the Macmillan Pass volcaniclastics. The Macmillan Pass volcaniclastics is an informal term that describes the carbonate-altered lapilli tuffs, tuffs, mafic flows, volcaniclastic breccias, sills, and dikes that are interbedded with the clastic rocks of the Earn Group (Turner and Rhodes, 1990; Ootes et al., 2013; Fraser et al., 2021). Turner and Rhodes (1990) constrained the volcanic rocks to Middle Devonian; however, interbedded volcanic layers are also observed in the underlying mudstones of the Duo Lake Formation.

The Niddery Lake Member comprises cherty and black siliceous radiolarian mudstones that occur with barite and limestone lenses that reach up to 30 m thick (Abbott, 2013). The overlying Macmillan Pass Member comprises three units (Gordey and Anderson, 1993), and at Macmillan Pass, there is lateral variability in lithofacies and thickness. The Member broadly consists of gray to black, thinly laminated silty mudstone that is finely interbedded with sandstones. A thick chert pebble conglomerate forms a continuous sequence with minor sandstone (Abbott, 2013). The Fuller Lake Member, previously called the Tom sequence (Abbott and Turner, 1991), is sandwiched between the Itsi Formation and the Macmillan Pass Member. The Member comprises a 200- to 1,500-m-thick succession of carbonaceous mudstones that are commonly pyritic (Goodfellow et al., 1990). Pyritized radiolarian tests have been identified in the Portrait Lake Formation mudstones, and the abundance of cryptocrystalline quartz has been linked with biogenic silica sourced from high levels of primary productivity in the basin (Magnall et al., 2015).

Sulfide mineralization in the Macmillan Pass district

In the Macmillan Pass district, Zn-Pb ± Ba mineralized rocks follow a 25-km trend defined by the Hess fault system that runs across the Macmillan fold belt (Abbott and Turner, 1991). The Tom and Jason deposits are ~5 km apart and comprise stratiform and stratabound sulfide mineralization. The Tom deposit is hosted in the Fuller Lake Member, whereas the Macmillan Pass Member hosts the Jason deposit. Feeder zone mineralization and alteration (ankerite, siderite, pyrite, sphalerite, and galena) are well preserved at both deposits, including stockwork, breccias, and veins with quartz and Fe carbonate-altered mudstones overlain by stratiform sulfide and barite-mineralized mudstones (Goodfellow et al., 1990; Magnall et al., 2016a).

Boundary Zone deposit

An earlier description of Boundary Zone (then Boundary Creek) suggested the mineralization formed in a subbasin consisting of carbonaceous and siliceous mudstones, cherty conglomerates, diamictites, and volcaniclastics (Turner and Rhodes, 1990). Abbott and Turner (1991) stated that the Boundary Zone sulfide mineralization may have formed synchronously with the stratiform mineralization at the Tom and Jason deposits and, therefore, represent the feeder zone facies of the SEDEX system. The mineralization was interpreted to be epigenetic, having formed below the sea floor due to fluid flow from syndepositional faults developed during the Late Devonian (Turner and Rhodes, 1990). Furthermore, the Boundary Zone mineralization was suggested to be genetically related to the regional alkaline volcanics (Turner and Rhodes, 1990; Abbott and Turner, 1991). A recent study by Scanlan (2022) on volcaniclastic rocks in the Selwyn basin, including samples from the Boundary Zone, indicates that alkaline magmatism may have contributed to sulfide formation by increasing the crustal heat flow and fluid circulation.

Methods

All analyses were carried out at the GFZ German Research Centre for Geosciences, Potsdam, Germany. A brief description of the methodology is provided below. For more detailed accounts of the techniques and analytical settings, the reader is referred to the supplementary data publication (Grema et al., 2024).

Sampling

A total of seventy-nine (79) samples for this study were collected from nine drill holes at Boundary Zone, comprising drill holes NB84-10, NB19-001, NB19-002, NB20-001, and NB20-002 in the eastern part and drill holes NB20-004, NB20-007, NB20-009, and NB21-001 in the western part (Fig. 3). The selected samples cover all the known mineralization and alteration styles and mineral assemblages. Seventy-three samples containing key mineral assemblages and paragenetic relationships were selected for petrographic and mineralogical investigation.

Petrography

Drill core samples were examined using a binocular microscope, and representative areas were selected for polished

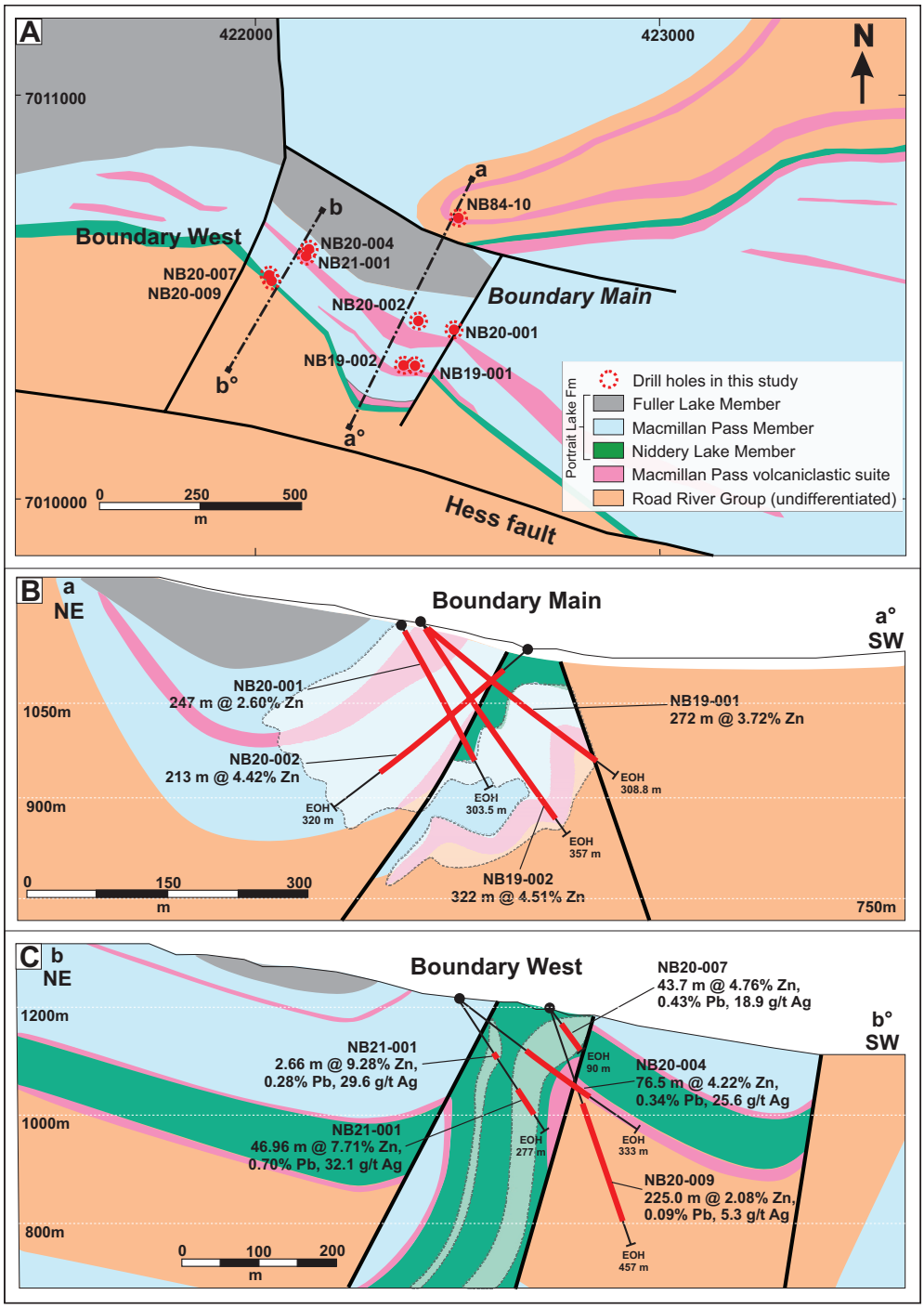

Fig. 3. (A) Geologic map of the Boundary Zone deposit area, with details of the drill holes sampled in this study. The Macmillan Pass Member units comprise the mudstones, conglomerates, and diamictites of Turner and Rhodes (1990). (B-C) Cross sections depicting mineralized sulfide intervals in the drill holes denoted by the red bar with outlines. The grades of Zn, Pb, and Ag are also shown (modified from Fireweed Metals Corp., 2021). EOH indicates the end of the hole.

thin section (~25-µm thickness) preparation (n = 80). A dual reflected- and transmitted-light Olympus BX51 polarizing microscope was used for detailed petrographic, textural, and mineralogical examination. A hot-cathode optical CL petrographic system was used to observe luminescence and zonation in sphalerite, fluorapatite, barite, and quartz from selected samples.

EPMA and SEM

Selected samples were carbon coated (20 nm thick) and analyzed using a field emission Japan Electron Optics Limited (JEOL) JXA-8530F Hyperprobe EPMA. Mineralogical, textural, and paragenetic relationships were examined using backscattered electron (BSE) imaging and electron disper-

sive spectroscopy (EDS) analysis. Mineral chemistry data by wavelength dispersive spectroscopy (WDS) were obtained using the EPMA equipped with a combined system of one energy-dispersive spectrometer and five wavelength-dispersive spectrometers. For fluorapatite mineral chemistry, the following oxides and elements were measured: P_2O_5, SiO_2, SO_3, Y_2O_3, La_2O_3, Ce_2O_3, Pr_2O_3, Nd_2O_3, CaO, MnO, MgO, FeO, Na_2O, SrO, F, and Cl. High-resolution BSE imaging and false color element distribution mapping of selected samples were performed using a Carl Zeiss Microscopy GmbH Ultra Plus field emission SEM.

SIMS U-Pb Geochronology

U-Pb age determinations of fluorapatite were performed using the large geometry CAMECA 1280-HR SIMS instrument. The analyses of the sample from the NB19-001 drill hole employed a Köhler $^{16}O_2^-$ primary beam between 4.3 and 7.3 nA. Data were acquired in monocollection mode using an ETP 133H electron multiplier and a mass resolution of M/ΔM ≈ 4,200 (at 10% peak height). The U-Pb fractionation factor was established using the Pb/U versus UO/U relationship, employing a power law fit as defined using reference material NW-1 with $^{206}Pb/^{238}U$ age of 1168.3 ± 4.5 Ma (Wu et al., 2017). Data reduction was performed with the help of the Excel-based program developed by Martin Whitehouse (NORDSIM facility, Stockholm), while the Isoplot package (version 4.15; Ludwig, 2012) was used for age calculation and data visualization. 1-σ notation in the processed data corresponds to the overall uncertainty of the measurement, including a run component (1 standard error) and a reference material component (1 standard deviation).

Quantitative X-ray diffractometry (QXRD)

A total of 73 samples were selected for QXRD, comprising 5- to 23-cm-long quarter cores from mineralized drill hole intervals (except for the NB84-10 drill hole, where barren and weakly mineralized cores were sampled). Milled samples were air dried, and randomly oriented powders analyzed using a PANalytical Empyrean X-ray diffractometer (XRD), using 40 mA, 40 kV, and Cukα radiation. A step size of 0.02o 2θ with 60 s/step was used from 4.6o to 85o 2θ. Preliminary mineral identification was conducted using the software EVA (Bruker, version 11.0.0.3). The software Profex (version 5.0.2; Doebelin and Kleeberg, 2015), calibrated for the PANalytical Empyrean XRD, was used for quantitative Rietveld refinement. Results are reported in percentages with an uncertainty of <3% for the quantitative analyses.

Results

Geology of Boundary Zone

Sulfide mineralized rocks at Boundary Zone are intersected over an area 2 km long, 200 to 800 m wide, and at depth between 20 and 300 m (Figs. 3, 4). The nine drill holes described in this study intersect stratigraphic units of the Road

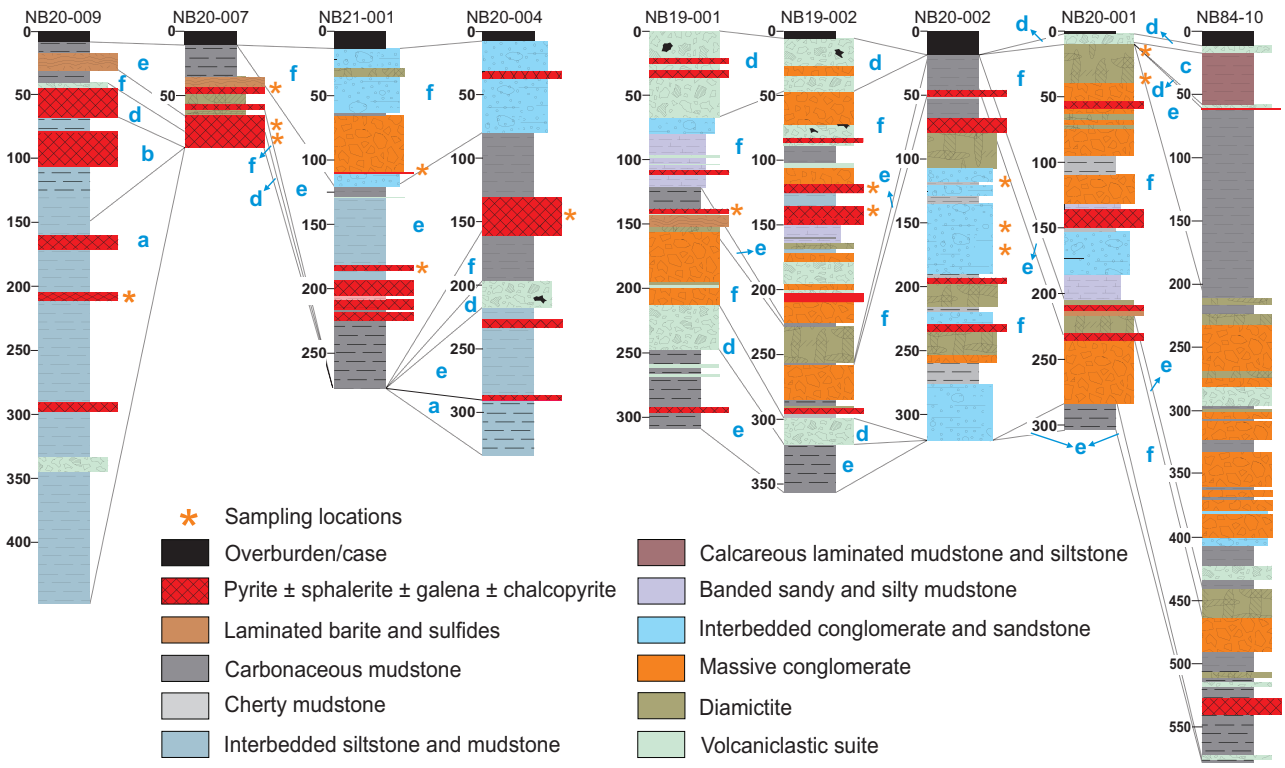

Fig. 4. Lithostratigraphic logs of the drill holes sampled in this study with sampling locations highlighted by the orange stars. Sulfide mineralized intervals are denoted by the red bars.

River Group (including the Duo Lake Formation and possibly Steel Formation) and the Portrait Lake Formation (Figs. 4, 5A-O). Both the Late Ordovician to Early Silurian Duo Lake and Middle to Late Devonian Portrait Lake Formations host Zn mineralization at Boundary Zone (Fig. 3B-C); however, the latter formation contains the majority of the sulfides. The mineralized rocks in both strata preserve two main paragenetic stages (Fig. 6) with stratabound sulfides in mudstones that are crosscut by veins, stockworks, and breccias (e.g., Fig. 7A).

Hand specimen and petrographic study of the host rocks

Duo Lake Formation: The Duo Lake Formation was intercepted in the NB20-009 drill hole (Fig. 4) and is the oldest unit sampled in this study, constrained by unpublished graptolite biostratigraphic data (M.J. Melchin, 2024, pers. comm.). The samples consist of gray to dark gray, finely laminated mudstones (Fig. 5A), which are variably cherty. Quartz forms a major part of the mineralogy and occurs as four main types (Fig. 6, classified based on Folk and Pittman, 1971). Detrital quartz (mostly <1 µm) is a relatively minor constituent and is dispersed in the matrix. Authigenic cryptocrystalline quartz (chalcedonic) and microquartz (grain sizes <20 µm) are the dominant phases. Megaquartz, with grain sizes >20 µm, forms mostly in veins or as pressure shadows around earlier mineral phases. The mudstones contain radiolarian-rich beds, often separated by mm- to sub-mm-thick layers of very fine grained, radiolarian-poor, clay-rich layers. The radiolaria tests are partially preserved by cryptocrystalline and microquartz (Fig. 5G) set in a cryptocrystalline quartz matrix containing microporosity (Fig. 5H) and pyrobitumen (App. Fig. A1I-J). Pyrite is finely disseminated in the mudstone matrix (Fig. 5H). Bedding-parallel and high-angle stylolites are observed within the mudstones, often forming both parallel to mudstone laminae and at the interface between the matrix and the radiolarian silicified tests (Fig. 5G).

Portrait Lake Formation: The Niddery Lake Member comprises rhythmically intercalated, cm-scale gray chert, pyrite, and dark gray to black, sometimes silty, mudstone layers (Fig. 5B). Mudstone layers vary in thickness from fine laminae (<10 mm) to beds up to 5 cm, giving the rock a banded appearance. The cherty layers comprise cryptocrystalline to microquartz (Fig. 5I) interbedded with layers that have radiolarian tests preserved by cryptocrystalline quartz, similar to the Duo Lake Formation (Fig. 5G). Notably, at certain stratigraphic intervals, the Niddery Lake Member mudstones comprise interbedded, carbonaceous, radiolarian-rich layers, bedded microquartz, and nodular barite crystals. Barite is finely disseminated in the matrix, with phyllosilicate minerals, primarily illite, and concentrated along laminae with differential compaction around the fluorapatite, barite, and pyrite mineral crystals (Fig. 5K).

The Macmillan Pass Member comprises intercalated mudstones, conglomerates, volcaniclastics, and diamictites. The mudstones have interbedded silty and black carbonaceous layers with fine-grained stratiform pyrite (Fig. 5C). The pyrite occasionally occurs as nodules and mm-sized grain aggregates. Subhedral to euhedral siderite crystals and minor dolomite are also disseminated in the mudstone matrix. Macmillan Pass Member interbedded conglomerates contain well-rounded to subangular, pebble-sized clasts of quartz, chert, and polylithic components (Fig. 5D). They can be clast supported or matrix supported, with quartz, siderite, and sulfide minerals in the cement.

Lapilli tuffs dominate the volcaniclastic beds that are interbedded with the Macmillan Pass Member (Fig. 4). The clasts in the tuff are subrounded to angular, varying in size from mm to a few cm, and exhibit hyaloclastic textures (Fig. 5E). Individual clasts and framework mineral grains in the lapilli tuffs are extensively altered and cemented by Fe carbonates and phyllosilicates (Fig. 5E, L).

The diamictites comprise a diverse mixture of unsorted mudstone, conglomerate, and volcanic clasts within a sand- to clast-supported matrix (Fig. 5F). Barite, fluorapatite, siderite, pyrite, celsian, and phyllosilicate minerals are common (Fig. 5M-N). Deformation features such as fractures, quartz veins, and dissolution seams (stylolites) are common in the diamictites (Fig. 5F, J).

Fig. 5. Representations of samples of the Boundary Zone host rocks highlighting the background mineralogical compositions. (A) Hand specimen photograph of dark gray siliceous mudstone of the Duo Lake Formation. Pyrite grains are rare and occur mostly as sparse disseminations. (B) Hand specimen photograph of the Niddery Lake Member comprising laminated mudstone and chert, with bedding-parallel pyrite layers. (C) Hand specimen photograph of finely laminated carbonaceous mudstone of the Macmillan Pass Member with rhythmic mm-scale pyrite-mudstone laminae. Coarse-grained pyrite and nodular grains are common. (D) Hand specimen photograph of a pebble-sized conglomerate of the Macmillan Pass Member. Clasts are mostly siliceous fragments, cherts, and mudstones. The cement commonly consists of quartz, siderite, and sulfide minerals. (E) Hand specimen photograph of Fe carbonate-cemented lapilli tuff with amygdular volcanic clasts. (F) Hand specimen photograph of a diamictite with different mudstone fragments supported in a pebble-to-sandy matrix. (G) Transmitted-light photomicrographs of Duo Lake Formation mudstone showing silicified radiolarian tests that have been preserved. (H) Backscattered electron (BSE) image of Duo Lake Formation with framboidal and subhedral pyrite set in a chert matrix. (I) Reflected- and transmitted-light composite photomicrograph of the Niddery Lake Member with disseminated framboids and coarser subhedral to euhedral pyrite. Bedding-parallel clay-rich layers are common. (J) Hand specimen photograph of black carbonaceous mudstone of the Niddery Lake Member, with stylolites (red arrows). (K) BSE image of siliceous mudstone of the Niddery Lake Member, showing patchy porous fluorapatite, barite, and pyrite. Dotted lines indicate differential compaction of the mudstone around the pyrite and fluorapatite crystals. (L) BSE image of diamictite with altered mudstone clast (left) and volcanic clast (right). Fluorapatite, phyllosilicates, and pyrite are common. (M) BSE image of a mudstone clast showing the phyllosilicate minerals, microcrystalline quartz, and K-feldspar. (N) BSE image of a mudstone clast of a diamictite, highlighting the replacement of barite by pyrite and celsian next to a trachytic volcanic clast (highlighted). (O) BSE image of a stylolite with fine-grained pyrite and phyllosilicate minerals. Abbreviations: Ap = fluorapatite, Bm = barian mica, Brt = barite, Cht = chert, Cls = celsian, Fe-carb. = iron carbonates, Ilt = illite, K-fs = potassium feldspar, Kln = kaolinite, Ms = muscovite, OM = organic matter, Phyll = phyllosilicate minerals, Py = pyrite, Qz = quartz, Qz_{cryp} = cryptocrystalline quartz, Qz_{mega} = megaquartz, Qz_{mic} = microquartz, Sd = siderite, Ser = sericite, Sp = sphalerite.

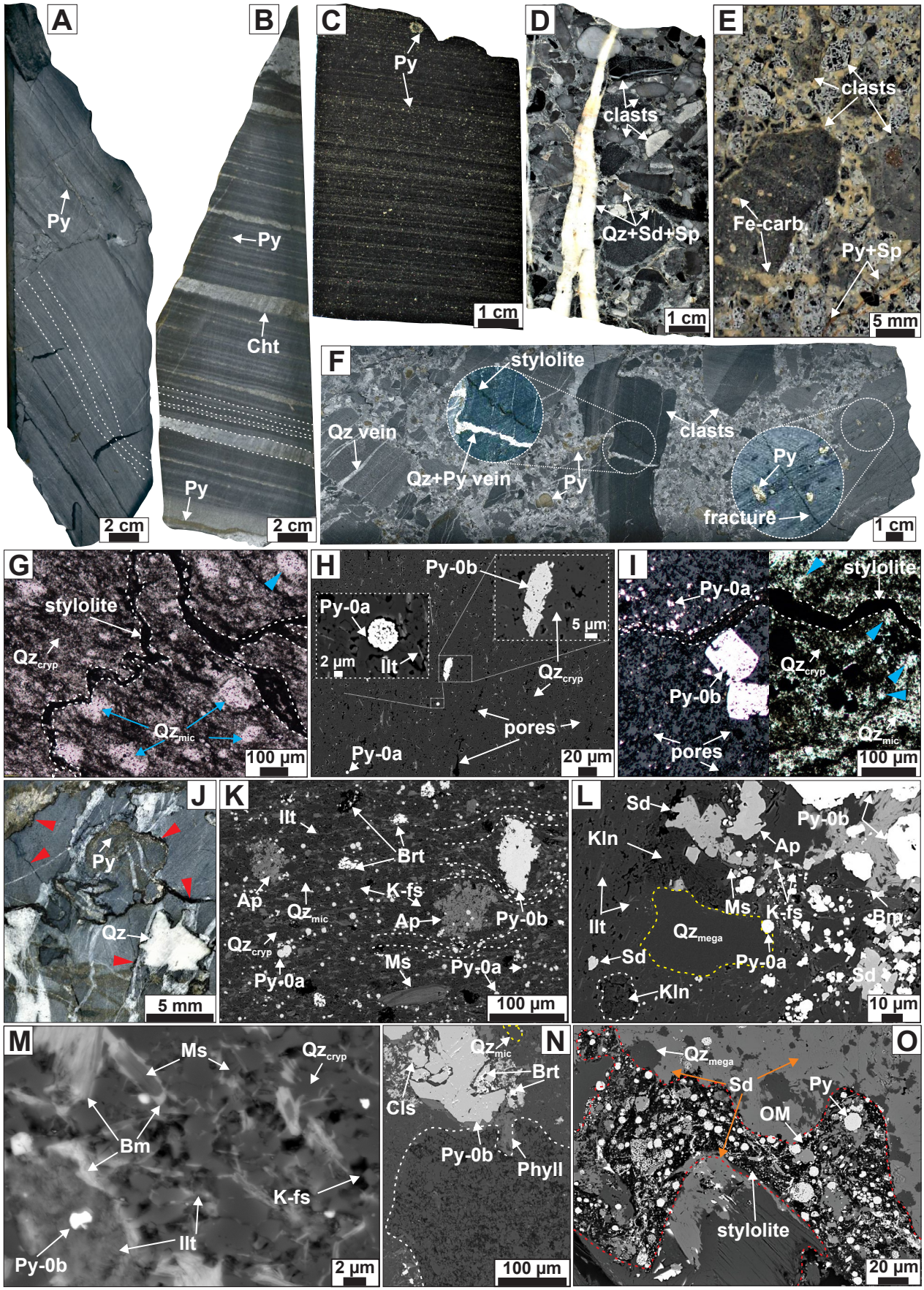

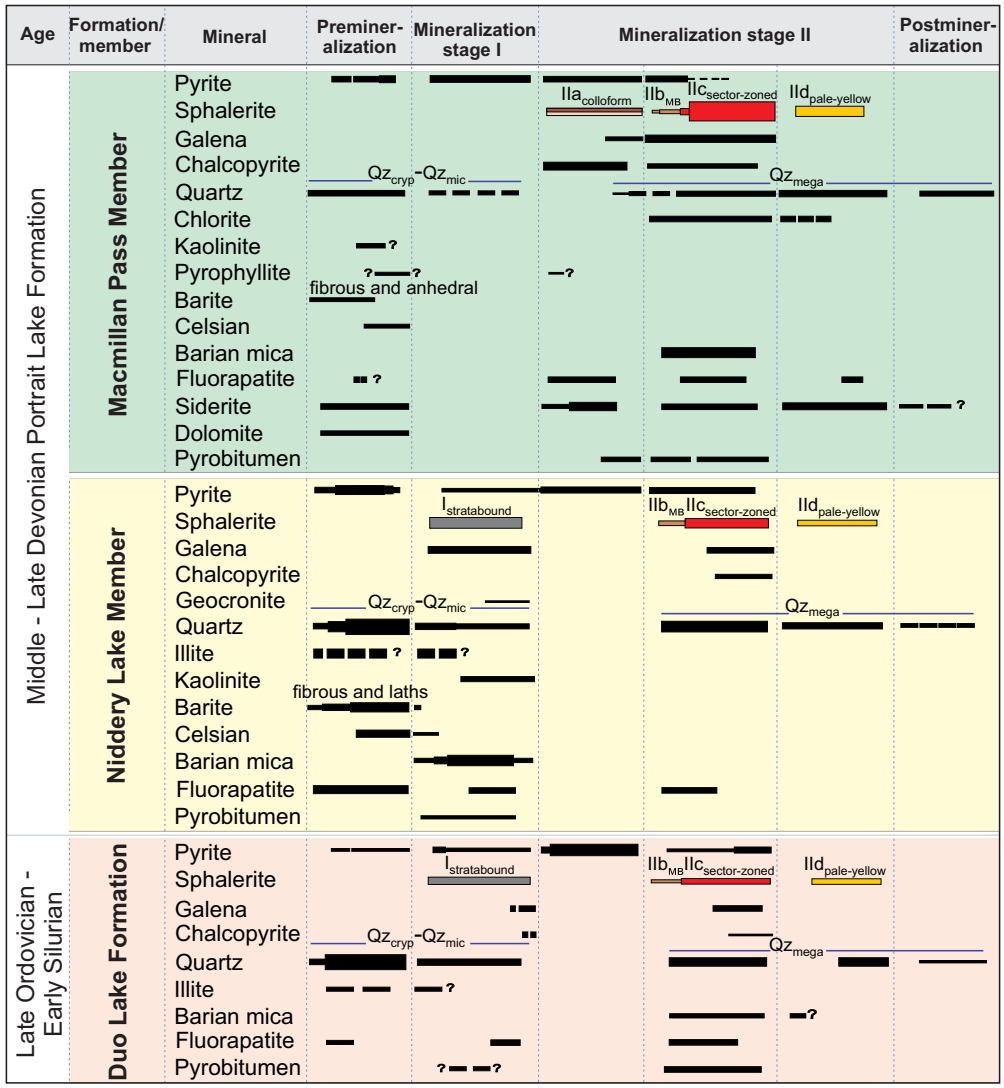

Fig. 6. Simplified paragenetic sequence for the Boundary Zone sulfides and other major mineral phases. Segmented bars indicate uncertain temporal formation of mineral occurrence. Bar thickness indicates the relative abundance of the mineral phases. The colored bars of the sphalerite represent the general colors of the grains. Abbreviations: MB = metallic brown, Qz_{cryp} = cryptocrystalline quartz, Qz_{mega} = megaquartz, Qz_{mic} = microquartz.

Paragenesis

Hand specimen identification, optical (transmitted- and reflected-light) microscopy, and EPMA techniques were combined to define a paragenesis comprising premineralization, mineralization stage I, and and mineralization stage II in the Duo Lake and Portrait Lake Formations. A summary of the paragenesis is given in Figure 6 and described below.

Premineralization stage: The premineralization stage in the Duo Lake and Portrait Lake Formations is characterized by the formation of two pyrite generations, quartz, barite, and phyllosilicate minerals. Premineralization pyrite (Py-0) comprises framboids (Py-0a) and anhedral to subhedral pyrite (Py-0b) that form in the interstitial pore spaces of the mudstones, concentrated along stratiform pyritic layers (e.g., Fig. 5B-C), or as disseminations in the matrices of mudstones, conglomerates, volcaniclastics, and diamictites. The Py-0a crystals are mostly <10 µm in diameter and can form aggregates that are up to 150 µm in size; whereas Py-0b crystals are relatively coarser grained (<120 µm) and often form an overgrowth on Py-0a.

In the Duo Lake Formation, Py-0a and b form as disseminated crystals in the mudstones but are relatively more abundant in the radiolarian-rich layers. Disseminated illite and organic matter are both abundant in the mudstones (Fig. 5H). In the Niddery Lake Member, Py-0a and b crystals are commonly concentrated along stratiform laminae in radiolarian-rich beds (Fig. 5I). Barite and fluorapatite are also commonly concentrated in the Niddery Lake Member mudstone (Fig. 5K).

The Macmillan Pass Member mudstone contains abundant Py-0a and b (Fig. 5C). These premineralization pyrites also formed in the Macmillan Pass Member conglomerate and diamictite, mostly occurring in the groundmass around the clasts (e.g., Fig. 5F). However, euhedral Py-0b crystals often rim the margins of the clasts in a replacive texture. In volca-

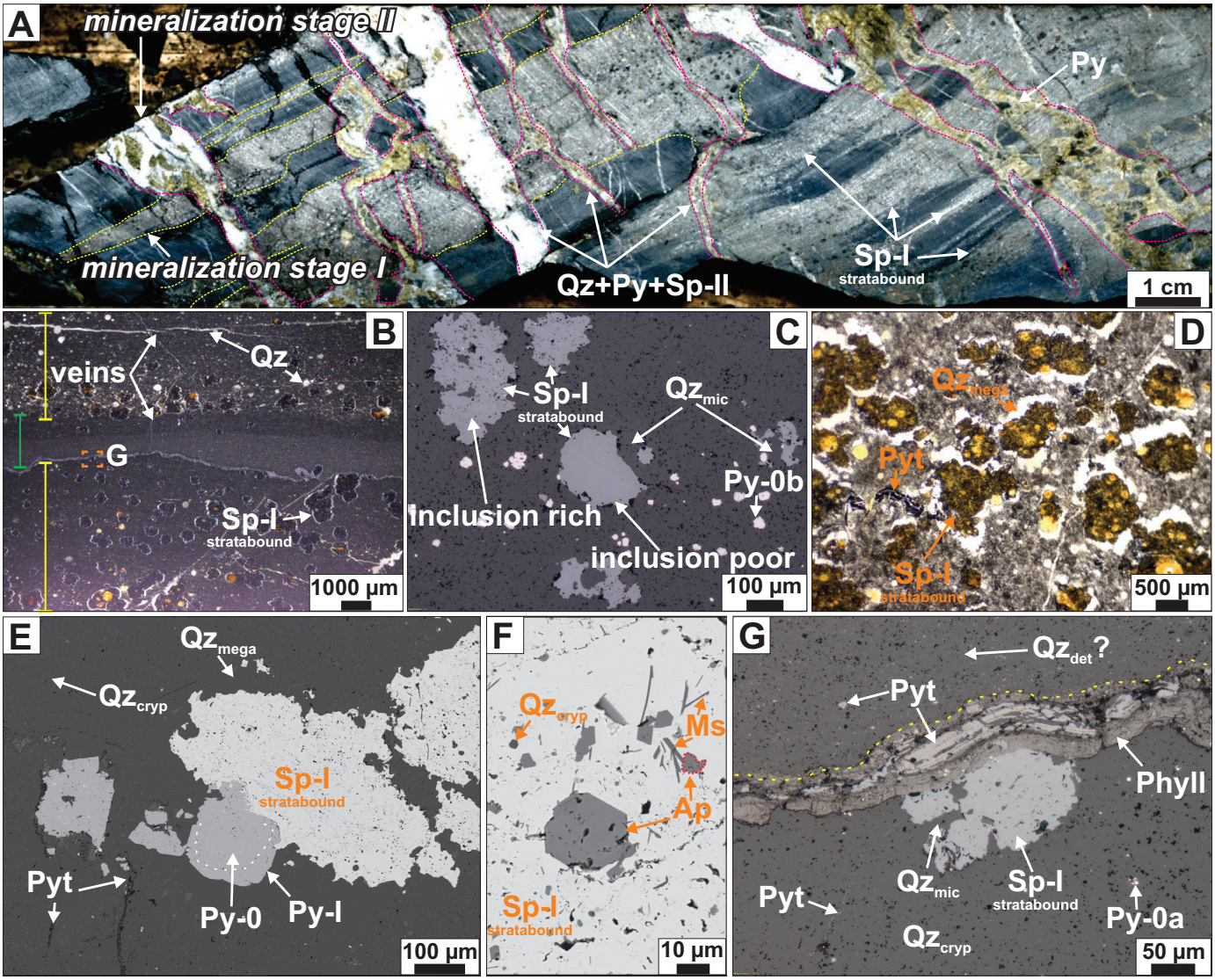

Fig. 7. Representation of stratabound sulfide mineralization in the Duo Lake Formation. (A) Photograph of siliceous mudstone sample showing bedding-parallel sphalerite layers crosscut by quartz and sulfide veins. (B) Binocular photomicrograph showing a dark gray mudstone layer separating two mineralized beds. (C) Reflected-light photomicrograph consisting of inclusion-rich and inclusion-poor sphalerite crystals. (D) Binocular photomicrograph of spherical sphalerite set in a cherty matrix. (E) BSE image of intergrown sphalerite and pyrite. Minor veinlets of pyrobitumen are present in the mudstone. (F) BSE image of subhedral to euhedral fluorapatite crystal intergrown with sphalerite. (G) Reflected-light photomicrograph of mineralization-stage I sphalerite (Sp-Istratabound) cut across by stylolite. Abbreviations: Ap = fluorapatite, Ms = muscovite, Phyll = phyllosilicate minerals, Py = pyrite, Pyt = pyrobitumen, Qz = quartz, Qz_{cryp} = cryptocrystalline quartz, Qz_{det} = detrital quartz, Qz_{mega} = megaquartz, Qz_{mic} = microquartz, Sp = sphalerite.

niclastics, subhedral to euhedral Py-0b is the volumetrically significant premineralization pyrite generation and forms crude laminae in the lapilli tuff. Porous celsian, subhedral fluorapatite, and phyllosilicate minerals (predominantly illite, kaolinite, pyrophyllite, and muscovite) form as part of the premineralization mineral assemblage in the volcaniclastics (Fig. 5L, N).

Mineralization stage I: The first mineralization stage comprises stratabound sphalerite, galena, and pyrite with minor chalcopyrite and sulfosalts. The sulfide minerals are hosted by the cherty and carbonaceous (silty) mudstones of the Duo Lake Formation (Fig. 7) and Niddery Lake Member of the Portrait Lake Formation (Fig. 8). Mineralization stage I sulfides are absent in the Macmillan Pass and Fuller Lake Members.

In the Duo Lake Formation, stratabound steel-gray sphalerite ($Sp\text{-}I_{stratabound}$) is disseminated or occurs in bedding-parallel, radiolarian-rich layers ranging from <1 mm to 50 cm thick (Fig. 7A-B). These mineralized beds are often interbedded with barren, very fine grained mudstone (Fig. 7B). $Sp\text{-}I_{stratabound}$ is broadly spherical and frequently forms pseudomorphic replacement of radiolarian tests, with grain sizes that range from <10 µm to 1.5 mm (Fig. 7C); it is associated with microquartz (Fig. 7D) and subhedral to euhedral crystals (Py-I) of pyrite (Fig. 7E). Minor anhedral galena, chalcopyrite, and subhedral

to euhedral, inclusion-rich fluorapatite are part of the assemblage together with pyrobitumen (Fig. 7D-F). The Sp-$I_{stratabound}$ crystals are often crosscut by pyrobitumen- and phyllosilicate-rich stylolites (Fig. 7G) that develop at the interface between mineralized and barren mudstone layers (Fig. 7B).

Stratabound sulfides in siliceous mudstone beds of the Niddery Lake Member are disseminated along bedding or occur in irregular layers of gray sphalerite (Sp-$I_{stratabound}$), galena (Gn-I), and pyrite (Py-I; Fig. 8). Here, Sp-$I_{stratabound}$ selectively and variably replaces radiolaria (Fig. 8B-C), barite (Fig. 8D-H), and the mudstone matrix (Fig. 8I-M), with crystal sizes ranging from <5 to 300 µm (e.g., Fig. 8B, G). In the radiolaria-rich beds, Sp-$I_{stratabound}$ forms with <130-µm-size aggregates of microquartz and megaquartz crystals that are surrounded by microquartz in the matrix (Fig. 8C). In contrast, in the barite-rich mudstone beds, anhedral Sp-$I_{stratabound}$ and Py-I form pseudomorphs of lath-like barite and the matrix (Fig. 8E). They commonly contain inclusions of barite (Fig. 8F) and premineralization Py-0a (Fig. 8G). Coarse-grained quartz and nodular Py-I are common in the matrix replacement intervals (Fig. 8I) where Sp-$I_{stratabound}$ often overgrows arsenic-rich Py-0a (Fig. 8J-M). The Gn-I crystals (<5 to 100 µm) occur with the other sulfides or in minor crosscutting veinlets (e.g., Fig. 8J). Silver-Sb-Pb–bearing sulfosalts, including tetrahedrite and geocronite (Geo; App. Fig. A2), are intergrown with Sp-$I_{stratabound}$ and Gn-I in the stratabound mineralized strata. Barian mica and kaolinite (Fig. 8H) are both associated with the mineralization stage I sulfides in the Niddery Lake Member.

Stylolites are present in mineralized and unmineralized Duo Lake and Portrait Lake Formations in bedding-parallel (e.g., Fig. 5I) and high-angle (e.g., Fig. 5G) forms. The stylolites in both barren and mineralized host rocks are characterized by dark seams that contain phyllosilicates, pyrobitumen, and pyrite (e.g., Fig. 5O). Notably, stylolites in mineralized samples from the Niddery Lake Member and Duo Lake Formation are observed to crosscut mineralization stage I (e.g., Fig. 7G). In the conglomerate of the Macmillan Pass Member, stylolitic margins are common features of the mineralization stage II mineralized veins, while such veins also truncate some stylolites (Fig. 9A inset).

Mineralization stage II: Brecciation and veining are prominent in the Duo Lake and Portrait Lake Formations. The breccias and veins that develop are infilled, and the fragments are cemented by sulfide minerals, phyllosilicates, megaquartz, and siderite (Figs. 7A, 9). The fragment sizes are variable and comprise mainly angular morphology with sharp contacts with the sulfides that occasionally fit together.

Mineralization stage II is the most volumetrically significant stage of sulfide formation at Boundary Zone and is best developed in the Macmillan Pass Member mudstones, conglomerates, volcaniclastics, and diamictites. Mineralization stage II style comprises layers, veins, and breccias (Fig. 9A-G) of sphalerite (four generations), pyrite, galena, and chalcopyrite, some of which crosscut the mineralization stage I stratabound sulfides (e.g., Fig. 7A). The major mineralization stage II gangue mineral phases are an assemblage of megaquartz, siderite, fluorapatite, and pyrobitumen.

Banded colloform sphalerite (Sp-$IIa_{colloform}$) mostly occurs in veins and breccias that are hosted by the Macmillan Pass Member (Fig. 9C-D), with the bands of crystals (<2.6 cm thick) formed at the margins of the wall rocks. Microscopically, Sp-$IIa_{colloform}$ comprises alternating bands (Fig. 9H) of dark brown to opaque and light brown to pale yellow crystals. Chalcopyrite occurs in the Sp-$IIa_{colloform}$ crystals as blebs (Fig. 9J) or as chalcopyrite disease. In contrast, minor galena (Gn-II) crystals are present as fine-grained inclusions, together with siderite and dolomite. Coarse-grained anhedral pyrite (Py-IIa) zones are sometimes intercalated with Sp-$IIa_{colloform}$ or form as anhedral to subhedral crystals in interstitial pore spaces of the Sp-$IIa_{colloform}$ (Fig. 9K). Py-IIa also forms massive layers in brecciated mudstones that commonly underlie the stratabound mineralization.

Two generations of coarse-grained sphalerite form overgrowths on Sp-$IIa_{colloform}$. These two sphalerite textures are not limited to the veins and breccias of the Macmillan Pass Member but are also common in the massive pyrite replacement layers that underlie the stratabound mineralization. Coarse-grained black to metallic brown sphalerite (Sp-$IIb_{metallic\text{-}brown}$) overgrows Py-IIa (Fig. 9B, E) and, rarely, the Sp-$IIa_{colloform}$ in the veins. Sp-$IIb_{metallic\text{-}brown}$ represents a minor component of the mineralization stage II sulfide assemblage. In transmitted light, Sp-$IIb_{metallic\text{-}brown}$ has a highly porous texture (Fig. 9L) and is intergrown with fine-grained euhedral pyrite crystals (<25 µm; Py-IIb) and aggregates.

The volumetrically dominant sphalerite generation at Boundary Zone consists of very coarse grained, up to 3-mm, red-brown sector-zoned sphalerite (Sp-$IIc_{sector\text{-}zoned}$, Fig. 9). Sp-$IIc_{sector\text{-}zoned}$ formed in veins that crosscut the Sp-$I_{stratabound}$ layers. In the veins, Sp-$IIa_{colloform}$ sphalerite is almost always overgrown by Sp-$IIc_{sector\text{-}zoned}$ (Fig. 9H). In contrast, in the breccia, Sp-$IIc_{sector\text{-}zoned}$ is abundant and sometimes the only sphalerite formed (e.g., Fig. 9G). Under transmitted light, Sp-$IIc_{sector\text{-}zoned}$ is occasionally rhythmically banded with red to colorless crystals (Fig. 9M). A coarse-grained (<1-cm) galena generation (Gn-II), which can grow up to 1 cm, is commonly intergrown with Sp-$IIc_{sector\text{-}zoned}$ in both veins (e.g., Fig. 9C) and breccias (e.g., Fig. 9G). Other coeval mineral phases include fluorapatite, pyrobitumen (Fig. 19C), and minor subhedral to euhedral megaquartz (Fig. 9N).

Finally, coarse-grained, pale-yellow to transparent sphalerite (Sp-$IId_{pale\text{-}yellow}$) is observed in the Duo Lake and Portrait Lake Formations. Sp-$IId_{pale\text{-}yellow}$ primarily postdates earlier sphalerite and pyrite generations (e.g., Fig. 9E) and infills cavities within the rocks (e.g., Fig. 9G). The individual crystals of Sp-$IId_{pale\text{-}yellow}$ range in size from 60 µm to mm-scale (Fig. 9H), and they are often associated with coarse, cm-scale megaquartz and siderite crystals in veins and breccias.

Fluorapatite chemistry

The premineralization, mineralization stage I, and mineralization stage II apatite crystals from Boundary Zone all plot in the fluorapatite region of the F-Cl-OH diagram (Fig. 10A), with median atoms per formula unit (apfu) F content of 2.54 (4.8 wt %; App. Table A1) and low Cl (Fig. 10B). Due to the beam-induced migration in EPMA analysis, the F content in these crystals is considered semiquantitative and exceeds the maximum content (~3.8 wt %) for stoichiometric fluorapatite (Piccoli and Candela, 2002). Broadly, there is a lack of system-

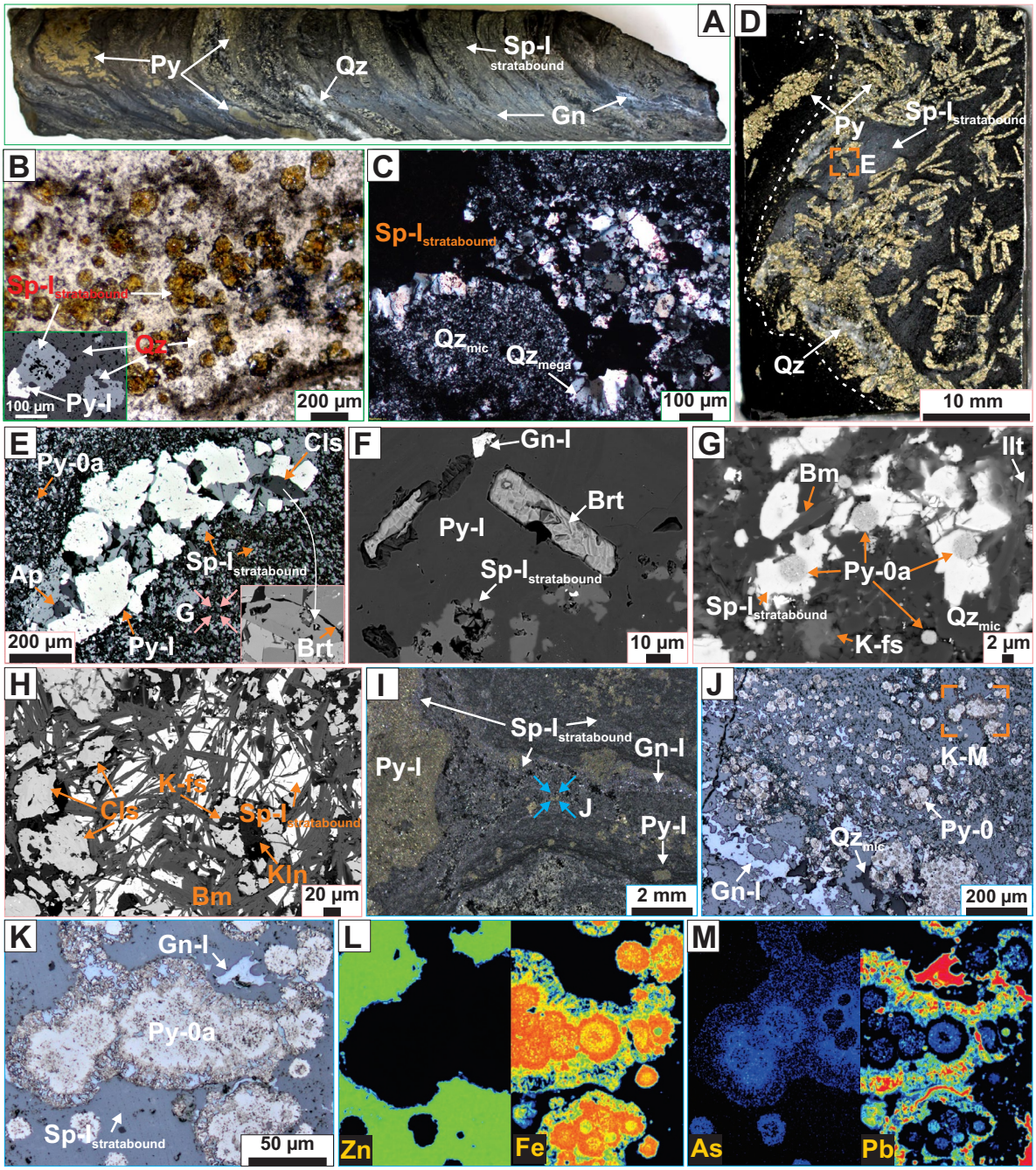

Fig. 8. Representation of stratabound (mineralization stage I) sulfides in the Niddery Lake Member of the Portrait Lake Formation. (A) Photograph of drill core; mineralized sample of the Niddery Lake Member. (B) Binocular photomicrograph of spherical sphalerite grains. Inset is a photomicrograph of intergrown sphalerite and pyrite with spherical morphologies. (C) Cross-polarized transmitted-light photomicrograph of intergrown coarser quartz with sphalerite. (D) Hand specimen photograph of mudstone highlighting the mineralization-host rock interface that shows the nature of replacement style sulfide formation. Pyritized laths are common in the mineralized region. (E) Reflected-light photomicrograph of the area highlighted in E. Sphalerite forms in the mudstone matrix and the laths, comprising pyrite, celsian, and fluorapatite. (F) Backscattered electron (BSE) image of barite laths with pyrite and sphalerite. (G) BSE image showing the nature of host-rock matrix replacement. Sphalerite primarily replaces and overgrow pyrite framboids. (H) BSE image of almost completely replaced mudstone with sphalerite, celsian, and barian mica. (I) Binocular photomicrograph of fine-grained sphalerite and pyrite grains set in mudstone that wraps around a pyrite nodule. (J) Reflected-light photomicrograph of a section similar to the highlighted area in I. Sphalerite and galena overgrow framboidal pyrite, almost entirely replacing the mudstone. (K) Reflected-light photomicrograph of the area highlighted in J. Pyrite framboids form the substrate for sphalerite and galena, set in the mudstone matrix. (L-M) Electron probe microanalysis (EPMA) element distribution map of the area in K, showing Zn and Fe (L) and As and Pb (M) composite maps. Abbreviations: Ap = fluorapatite, Bm = barian mica, Brt = barite, Cls = celsian, Gn = galena, Ilt = illite, K-fs = potassium feldspar, Kln = kaolinite, Py = pyrite, Qz = quartz, Qz_{mega} = megaquartz, Qz_{mic} = microquartz, Sp = sphalerite.

atic variation in Sr, Mn, and rare earth element (REE)+Y (La + Ce + Pr + Nd + Y) contents (Fig. 10C-D), except for higher Si content in the premineralization fluorapatite (likely due to background contamination/inclusions) and lower Sr (<1 wt %) in the fluorapatite coeval with Sp-IIa$_{colloform}$. In contrast, the Duo Lake Formation (median = 1.9 wt % Sr and up to 9.4 wt %) and Niddery Lake Member host fluorapatite with elevated Sr contents. A minor negative correlation exists between Ca and Sr, Mn, and REE + Y (Fig. 10D).

Fluorapatite U-Pb geochronology

Premineralization, mineralization stage I, and mineralization stage II fluorapatite crystals were analyzed for U-Pb dating; however, most crystals had high nonradiogenic Pb contents and low U mass fractions, making a reliable age determination impossible. The only successful dating was produced on fluorapatite crystals in a vein crosscutting mineralization stage I (NB19-001 drill hole). All fluorapatite U-Pb results (App. Table A2), together with preanalysis and postanalysis images (App. Figs. A4, A5) of the crystals, are provided in Grema et al. (2024).

A total of fourteen measurements were produced on crystals in NB19-001, although eight of these results were rejected due to cracks, abundant inclusions, and/or porosity. Three of the remaining analyses did not show crater-related issues, while in the other three, there were some inclusions and porosity that could have potentially influenced U-Pb determinations. In the end, all six analyses were taken into account due to the fact that the data reduction yielded similar ^{207}Pb-corrected ages, with the weighted mean of 169 ± 10 Ma (2 σ, mean square of weighted deviates [MSWD] = 0.54; Fig. 10E-F). Given the complexity of the studied samples and general challenges related to U-Pb dating of minerals of the apatite supergroup, which commonly incorporate nonradiogenic Pb into the structure (e.g., Pan and Fleet, 2002), we were unable to rigorously constrain the uncertainties of our measurements. Therefore, based on the SIMS data obtained for six fluorapatite grains in veins hosted in the Niddery Lake Member (Table 1), we assign a Middle Jurassic formation age for the fluorapatite.

QXRD mineralogy

The QXRD data are part of appendix table A3 in Grema et al. (2024) and are featured in Figure 11. The NB84-10 drill hole, which primarily intersects the Macmillan Pass Member units, is unmineralized (apart from two samples containing 1–4% sphalerite) and is referred to as barren in the following section. The major groups of mineral phases from the QXRD data are summarized by host rock types. The whole-rock mudstone mineralogy plots dominantly in the siliceous mudstone and siltstone field of the quartz + feldspar-phyllosilicate-carbonate ternary diagram (Fig. 12A).

Duo Lake Formation: Samples from the Duo Lake Formation mudstones are significantly enriched in quartz (mean = 64%), apart from massive sulfide samples (minimum = 8%; Fig. 11A). Fluorapatite is a minor component in most samples (~1%), although one brecciated sulfide-rich sample has ~5% fluorapatite. Pyrite and sphalerite are the main sulfide minerals, with pyrite mostly concentrated in breccias and veins (16–77%) compared to 1 to 21% observed in stratabound mineralization with sphalerite. The highest sphalerite abundances are hosted in stratabound layers (3–18%) rather than ≤2% in the breccias and veins.

Portrait Lake Formation: Lapilli tuff samples (n = 4) comprise ≤24% quartz (one quartz vein sample with 52%) with relatively high siderite (11–42%), illite (1–14%), and pyrophyllite (<1–15%) in the barren samples. One lapilli tuff sample (H1926) contains sulfide mineralization with 51% sphalerite, 2% chalcopyrite, and <1% pyrite.

In the Niddery Lake Member, quartz abundance varies from <25% in the massive sulfide mineralized samples to 83% in the weakly stratabound sulfide mineralized samples. Pyrite (1–85%) and sphalerite (<1–61%) are the dominant sulfide minerals. The Niddery Lake Member mudstones have the highest proportion of galena, reaching 14%, with minor chalcopyrite (0–3%) in multiple samples.

Fig. 9. Representation of mineralization stage II sulfide formation. Mineralization forms in massive sulfide layers, veins, stockwork, and breccias. (A) Drill core photograph of mineralization stage II sulfide interval in NB19-001 drill hole; 110.1–119.95 m. The mineralization in the hanging wall increases significantly toward the fault. Inset is a hand specimen photograph of a mineralized conglomerate. Sulfide veins appear intimately related to stylolites that also host sulfide minerals. Both barren (red arrows) and mineralized (yellow arrows) stylolites are shown. (B) Hand specimen photograph of massive sulfide mineralization with multiple sphalerite generations and late-stage quartz. (C) Hand specimen photograph of a vein with three sphalerite generations. Colloform sphalerite forms at the margins of the vein. Galena, quartz, and siderite are common in the later sphalerite generations. (D) Photograph of vein-hosted coarse-grained sulfide mineralization in the Macmillan Pass Member conglomerate. Early vein sphalerite consists of a colloform texture overgrown by coarse-grained red-brown sphalerite. Centimeter-scale euhedral quartz and siderite fill in the cavities in the veins. (E) Hand specimen photograph of massive sulfide sample with pyrite and three generations of sphalerite. Colorless quartz appears intergrown with pale yellow late sphalerite. (F) Hand specimen photograph of sulfide-mineralized lapilli tuff with sphalerite; siderite vein. The host rock is cemented by siderite, pyrite, and minor quartz. (G) Hand specimen photograph of brecciated Macmillan Pass Member mudstone. Mudstone fragments are preserved within the sulfides in the breccia. (H) Thin section photograph of banded colloform sphalerite overgrown by later sphalerite generations. (I) Backscattered electron (BSE) image of a vein mineral assemblage in the Duo Lake Formation, consisting of sphalerite, pyrite, fluorapatite, pyrobitumen, quartz, and barian mica. (J) Reflected-light photomicrograph of colloform sphalerite with chalcopyrite blebs. (K) BSE image of sphalerite, galena, and siderite dolomite intergrowth. Note the porosity around the anhedral pyrite aggregates and euhedral siderite crystals. (L) Reflected-light photomicrograph showing two generations of sphalerite: highly porous sphalerite and crystalline euhedral sphalerite intergrown with quartz. (M) Transmitted plane-polarized light photomicrograph highlighting the relationship between sector-zoned sphalerite and the pale yellow sphalerite that forms an assemblage with quartz. (N) Cathodoluminescence photomicrograph of a massive sulfide sample. A late-stage barite vein crosscuts pyrite and sphalerite. Abbrviations: Ap = fluorapatite, Bm = barian-mica, Brt = barite, Ccp = chalcopyrite, Dol = dolomite, Gn = galena, Py = pyrite, Pyt = pyrobitumen, Qz = quartz, Sd = siderite, Sp = sphalerite.

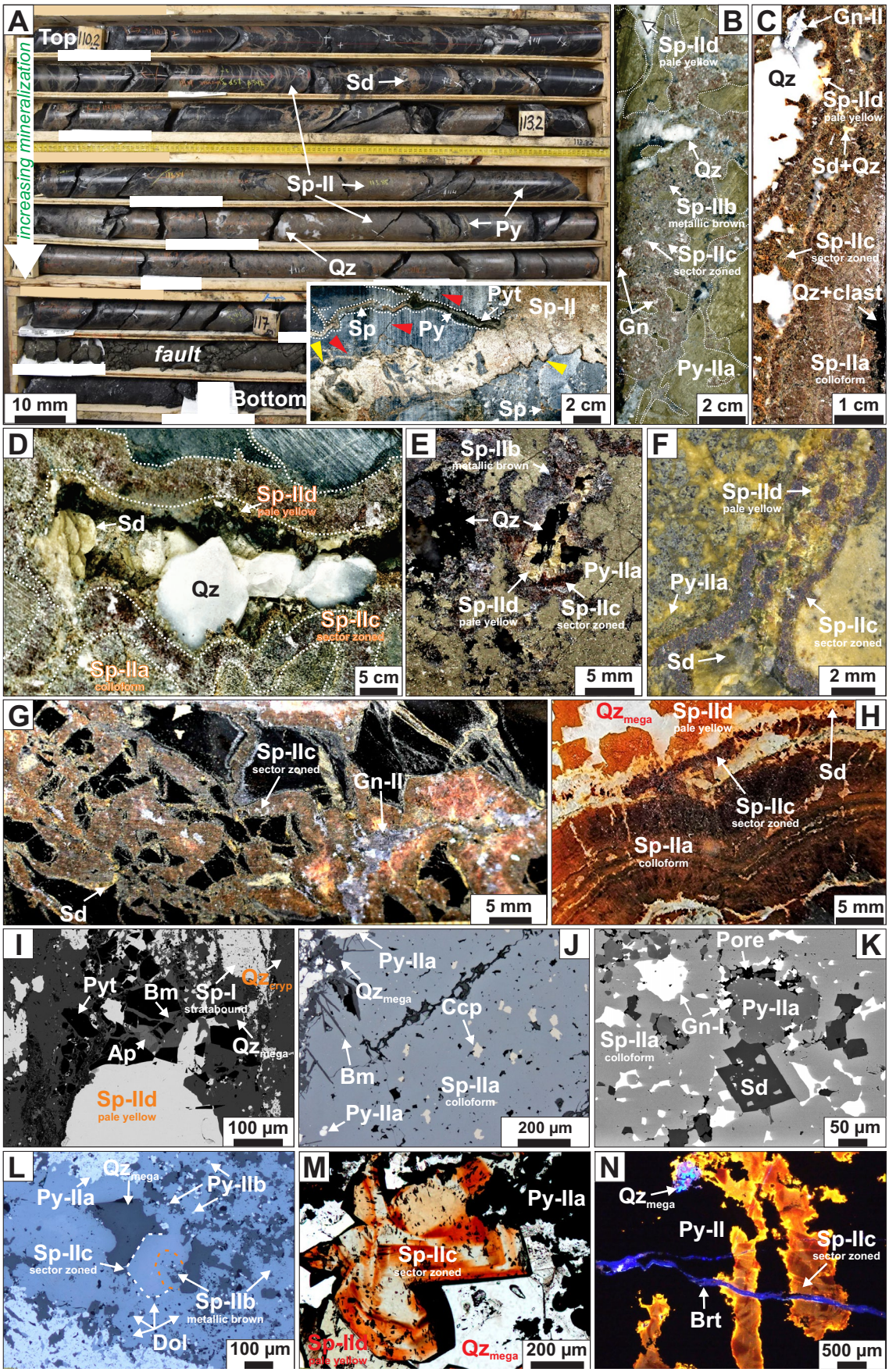

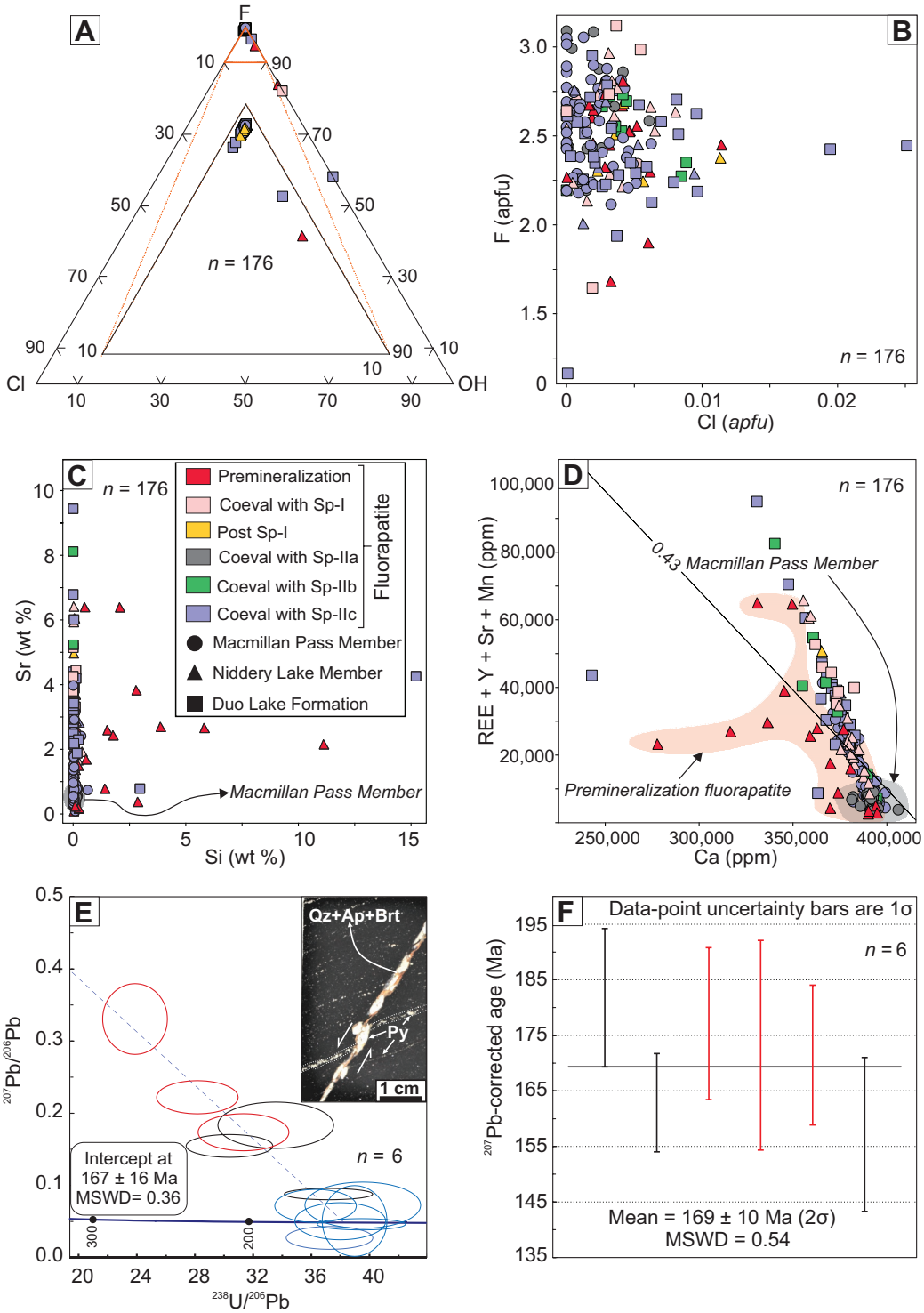

Fig. 10. (A) Fluorapatite F-Cl-OH ternary diagram of the major halogen composition. Inset is an enlarged part of the diagram indicated in orange color. (B) Binary plot of Cl vs. F calculated to atoms per formula unit (apfu) on the basis of 26 oxygen atoms in fluorapatite obtained via electron probe microanalysis (EPMA). (C) Binary plot of Si vs. Sr (wt %). (D) Binary plot of Ca vs. ΣREE + Y + Sr + Mn (in µg/g). ΣREE = La + Ce + Pr + Nd. REE = rare earth elements. (E) Total Pb/U isochron (a three-dimensional $^{238}U/^{206}Pb$ vs. $^{207}Pb/^{206}Pb$ vs. $^{204}Pb/^{206}Pb$ plot) showing the secondary ion mass spectrometry (SIMS) fluorapatite geochronology results from postmineralization stage veins in the Niddery Lake Member mudstone at Boundary Zone (n = 6). Inset is the Niddery Lake Member sample with the dated fluorapatite in a discordant vein. (F) ^{207}Pb-corrected age (weighted mean) for the six postmineralization fluorapatite crystals, with data point uncertainties indicated as 1σ. Black circles and bars in E and F indicate measurements without inclusions. Red circles and bars indicate measurements with potential influence from inclusions and pores. See data publication for detailed descriptions (Grema et al., 2024). Abbreviations: Ap = fluorapatite, Brt = barite, MSWD = mean square of weighted deviates, Qz = quartz, Sp = sphalerite.

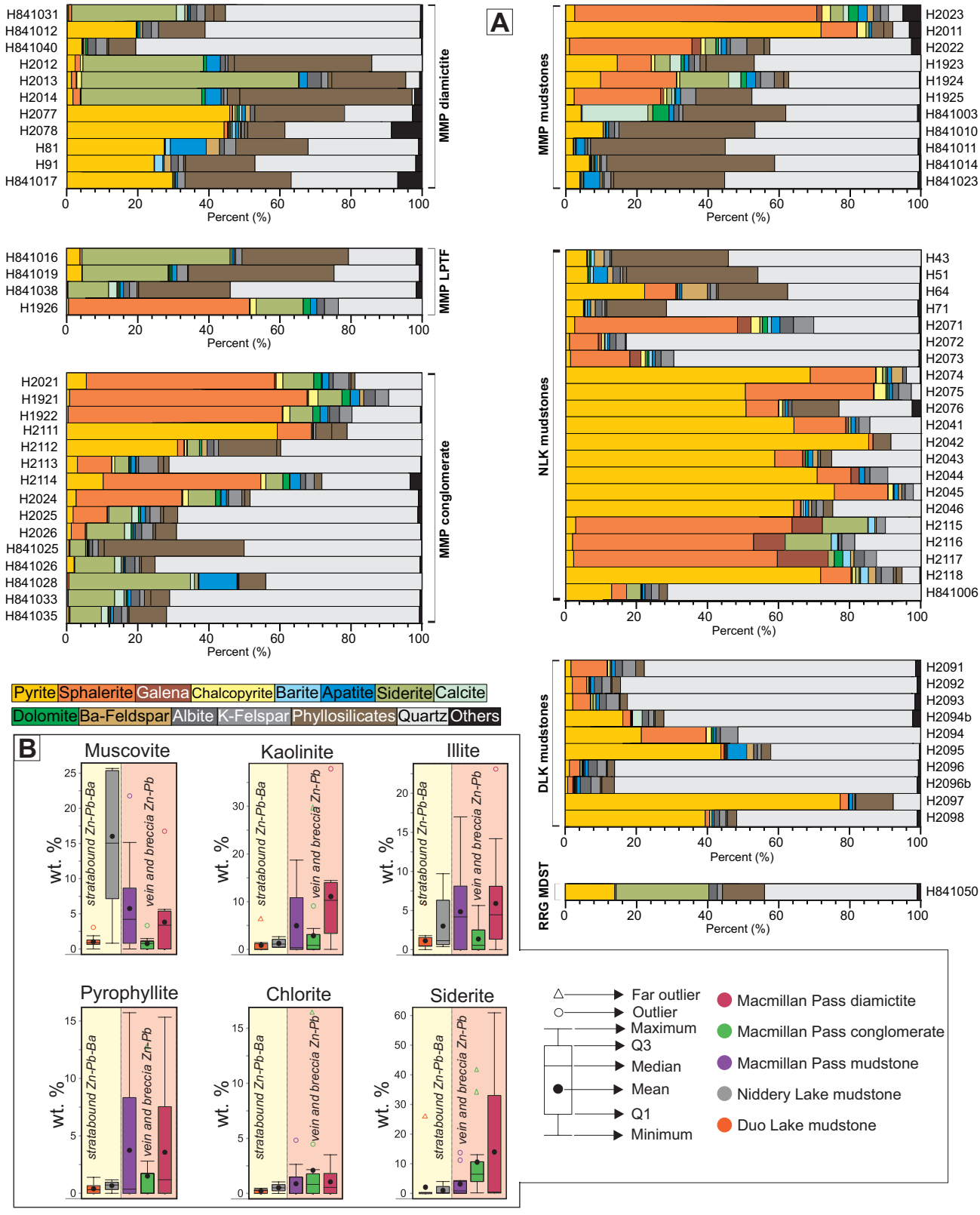

Fig. 11. Results of quantitative X-ray diffraction (QXRD) and clay-size X-ray diffraction (XRD) analyses of samples from Boundary Zone. (A) Stacked backplots of QXRD results showing the mineralogical composition of selected samples. (B) Box and whisker plots of dominant phyllosilicate mineral phases in the host rocks, sorted by the sulfide mineralization style. Siderite is common and comprises a significant component of the Macmillan Pass Member. Abbreviations: DLK = Duo Lake Formation, LPTF = Lapilli tuff, MDST = Mudstone, MMP = Macmillan Pass Member, MXSX = Massive sulfides, NLK = Niddery Lake Member, RRG = Road River Group, VCDM = Volcaniclastic diamictite.

Table 1. SIMS U-Pb Fluorapatite Data for Sample a5 From a Vein Crosscutting Mineralization Stage I

Sample name	Analysis ID	$^{207}Pb/^{206}Pb$	1 SE (%)	$^{208}Pb/^{206}Pb$	1 SE (%)	$^{204}Pb/^{206}Pb$	1 SE (%)	$^{206}Pb/^{238}U$	1 SE (%)	$^{238}U^{16}O/^{238}U$	1 SE (%)
H42	a5_Ap_Vein_2	0.1547	6.7	0.2841	11.0	0.0078	26.0	0.12	3.9	6.36	1.1
H42	a5_Ap_Vein_4	0.0880	5.9	0.1012	10.3	0.0026	32.2	0.10	2.5	6.37	0.7
H42	a5_Ap_Vein_8	0.2221	6.8	0.4679	8.6	0.0092	28.0	0.12	3.9	6.21	1.6
H42	a5_Ap_Vein_9	0.3305	9.8	0.8037	12.6	0.0172	26.8	0.16	4.9	6.37	1.6
H42	a5_Ap_Vein_11	0.1737	9.7	0.2718	13.9	0.0076	31.9	0.13	4.1	6.57	1.4
H42	a5_Ap_Icl_1	0.1834	11.5	0.3067	13.5	0.0068	49.9	0.12	4.8	6.52	1.4

Notes: Columns $^{207}Pb/^{206}Pb$, $^{208}Pb/^{206}Pb$, $^{206}Pb/^{238}U$, $^{238}U^{16}O/^{238}U$, $^{232}Th^{16}O/^{238}U^{16}O$, $^{40}Ca^{231}P^{16}O_4/^{238}U$, $^{206}Pb/^{238}U^{16}O$, ^{206}Pb/Coeff, and ^{204}Pb/Coeff contain measured data; please refer to the data publication for the complete data set
Abbreviations: Ap = fluorapatite, SIMS = secondary ion mass spectrometry

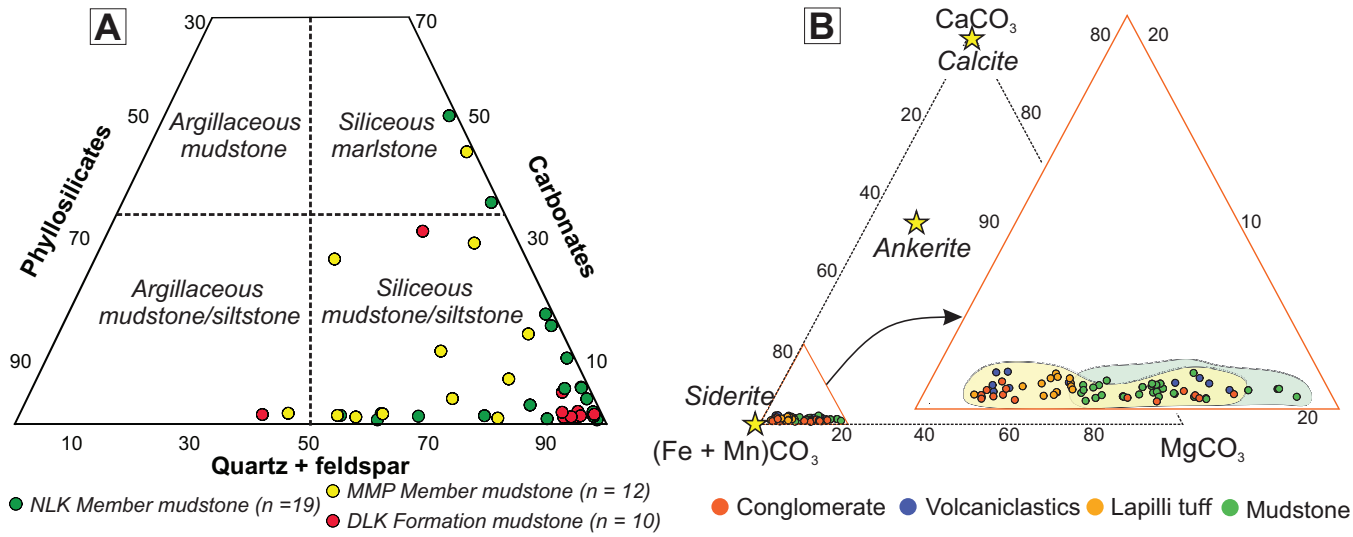

Fig. 12. (A) Mudstone quantitative X-ray diffraction (QXRD) compositional data of the Duo Lake and Portrait Lake Formations plotted in a quartz + feldspar-phyllosilicates-carbonate ternary plot. (B) Ternary plots of siderite mineral chemistry from electron probe microanalysis (EPMA). Magnesium-rich siderite grains are relatively enriched in the mudstones (App. Fig. A2). Abbreviations: DLK = Duo Lake Formation, MMP = Macmillan Pass Member, NLK = Niddery Lake Member.

In the barren Macmillan Pass Member mudstones, quartz varies between 37 and 75%, compared to 4 to 47% (mean = 35%) in the mineralized samples. Except in two samples where dolomite (5%), calcite (19%), and siderite (11%) occur in the barren mudstones, the mineralized samples are typically more enriched in carbonates with siderite (1–14%) and minor dolomite and calcite (<3%). Barren mudstones contain illite (2–17%), pyrophyllite (<1–16%), and muscovite (1–22%), in contrast to their minor presence (<1%) in the mineralized samples; muscovite is the exception, with one sample up to 15%.

The Macmillan Pass Member conglomerate unit has similar quartz content in the barren and mineralized samples, where barren samples contain 4 to 34% siderite compared to <1 to 11% in mineralized samples. Illite (1–6%), muscovite (1–3%), and pyrophyllite (2–13%) are higher in the barren conglomerates compared to <3% in the mineralized samples, which contain sphalerite (up to 67%) and chalcopyrite between 1 and 3%. The Macmillan Pass diamictite, with clasts, volcaniclastic rocks, conglomerate, and mudstone, has the lowest bulk quartz content (mean = 20%), but high siderite (up to 61%), illite (<1–23%), kaolinite (<1–38%), and fluorapatite (<1–10%). Compared to other rock types, diamictite has the lowest sphalerite (between <1 and 10%) but high pyrite (between 1 and 72%).

Discussion

The formation of sulfide mineralization at different stratigraphic levels at Boundary Zone provides a unique cross section of mineralizing processes in a classic CD-type district. In the following discussion, petrographic observations are combined with bulk mineralogy (QXRD) to develop a paragenetic model for the Boundary Zone system that can be compared with related systems in the Selwyn basin (e.g., Howards Pass district and the neighboring Tom and Jason deposits).

Host-rock composition and diagenesis

The stratigraphic units that host the sulfide mineralization at Boundary Zone are highly siliceous (Figs. 5, 11), similar to host units in the Howard's Pass (Morganti, 1979) and Macmil-

$^{232}Th^{16}O/^{238}U^{16}O$	1 SE (%)	$^{40}Ca^{231}P^{16}O_4/^{238}U$	1 SE (%)	^{206}Pb/Coeff	1 SE (%)	$^{206}Pb/^{238}U^{16}O$	1 SE (%)	^{204}Pb/Coeff	1 SE (%)	^{207}Pb corrected age (Ma)	1 σ (Ma)
0.00	34.7	2712	4.9	14	3.4	0.02	3.8	0.11	25.8	182	12
0.00	22.3	967	2.9	29	4.1	0.02	2.5	0.08	33.8	163	9
0.02	6.9	2152	5.5	11	3.8	0.02	3.8	0.10	27.7	177	14
0.01	16.7	4382	3.3	8	4.5	0.02	5.2	0.13	25.6	173	19
0.00	17.2	2743	1.6	10	4.0	0.02	4.1	0.08	31.6	171	13
0.00	28.5	3750	5.7	7	4.7	0.02	4.8	0.05	50.7	157	14

lan Pass districts (e.g., McClay, 1991; Magnall et al., 2015), and more broadly the Red Dog district in Alaska (Dumoulin et al., 2004).

At Boundary Zone, the cryptocrystalline and microquartz in the mudstones are concentrated in beds that also preserve spherical to elliptical "ghosts" of former radiolarian tests (Fig. 5G). The abundance of radiolarian ghosts in the sequence suggests there was a potentially significant flux of biogenic silica (as opal-A) during host-rock deposition, consistent with previous work in the Macmillan Pass district (Magnall et al., 2015). Importantly, the physical properties of biosiliceous mudstones are influenced by diagenetic transformations of opaline silica. Specifically, the transformation of opal-A to opal-CT (cristobalite and tridymite) results in a volume change and typically occurs at 40° to 50°C, corresponding to depths of ~100 to 1,000 m (Potter et al., 2005). This change includes volume reduction and release of water from the sediments. The conversion of opal-CT to authigenic quartz then occurs at relatively higher burial temperatures (60°–90°C; Weller and Behl, 2017). Notably, the volume change associated with opaline silica diagenesis can result in inherited microporosity within authigenic quartz (Milliken and Olson, 2017), as preserved in the cryptocrystalline and microquartz (e.g., Fig. 5H), which may have provided more permeable pathways in the sediments for subsequent fluid flow. Furthermore, there is increase in the tensile strength of siliceous mudstones cemented by microquartz that also impact on the brittle nature of the rocks (Milliken and Olson, 2017).

Barite, pyrite, and fluorapatite formation

The evidence of differential compaction of the surrounding host rock during the formation of barite and fluorapatite (e.g., Fig. 5K) and Py-0a and b in both the Duo Lake and Portrait Lake Formation mudstones (Fig. 5K) is consistent with formation during early diagenesis (e.g., Paytan et al., 2002; Canet et al., 2014; Salama et al., 2018).

At Boundary Zone, the Niddery Lake Member hosts the volumetrically major bedded barite, albeit at a different stratigraphic position from nearby occurrences. For example, stratiform barite formed during the Frasnian at the Tom and Jason deposits (Fuller Lake and Macmillan Pass Members; Carne, 1979; Turner, 1986; Goodfellow et al., 1993) and in the uppermost mudstones of the Canol Formation regionally (Fernandes et al., 2017; Grema et al., 2022). The differences in stratigraphic level, volume, and textures of barite between Boundary Zone and these locations may suggest the occurrence of another barite-bearing interval in the Macmillan Pass district. This horizon within the Givetian Niddery Lake Member (Abbott, 2013) at Boundary Zone may be correlative with the reported Road River-Canol Formation boundary unit of Fraser and Hutchison (2017) and the hyperenriched black shales (HEBS) reported across the Selwyn basin and part of the Richardson trough (Gadd et al., 2020). Notably, significant barite formation (up to 62% from XRD analysis) is reported within this horizon in the Yukon (Fraser and Hutchison, 2017; Kabanov, 2019) and has been linked to a period of anoxic sedimentation of carbonaceous sediments in the Selwyn basin (Kabanov, 2019).

Diagenetic barite formation results from fluid mixing at a major redox boundary, where highly reducing methane and barium-rich fluids mix with sulfate in shallower pore fluids (Torres et al., 2003). This redox boundary is known as the sulfate methane transition zone and is also an important location of diagenetic pyrite formation due to sulfate reduction coupled with the anaerobic oxidation of methane (SR-AOM; Gonzalez-Muñoz et al., 2012; Carter et al., 2020). Importantly, pyrite formation at a premineralization sulfate methane transition zone has been suggested in both the host rocks in the Howards Pass and Macmillan Pass districts (Magnall et al., 2016b; Johnson et al., 2018). The premineralization pyrite-barite assemblage reflects diagenetic processes that enriched the host rock in sulfur (Fig. 2C), providing an effective metal trap during host-rock replacement (Fig. 2D; Magnall et al., 2020).

Fluorapatite: Fluorapatite formed in the premineralization stage and mineralization stages I and II in the Duo Lake and Portrait Lake Formations. Fluorapatite is a common phase in CD-type deposits and has been described in premineralization and mineralization stages, as well as during recrystallization of existing apatite minerals (e.g., Red Dog District, Slack et al., 2004b; Howard's Pass district, Gadd et al., 2016a). The negative correlation observed in Figure 10D likely reflects the substitution of Sr, Mn, and REE + Y for Ca. The highest Si content is observed in the porous premineralization fluorapatite hosted in the siliceous Niddery Lake Member. This premineralization fluorapatite is suggested to have formed during early diagenesis together with barite. The elevated Si content may reflect the abundance of silica during fluorapatite precipitation, and elevated SiO_2 observed in the EPMA analysis could have resulted from background contamination and/or quartz inclusions (Fig. 5K). The common occurrence of fluorapatite in the mudstones suggests high primary produc-

tivity as authigenic apatite formation during diagenesis likely resulted from significant burial of P associated with organic matter decomposition (Berner et al., 1993).

Timing and style of mineralization stage I

Mineralization stage I sulfides in the Duo Lake Formation and Niddery Lake Member formed by stratabound replacement of the biosiliceous mudstone, resulting in overgrowth of preexisting diagenetic Py-0a and b (e.g., Fig. 8G). The selective mineralization of radiolarite beds (e.g., Figs. 7B, 8B) suggests fluid flow was focused along these particular intervals. The coexistence of Sp-$I_{stratabound}$, cryptocrystalline quartz, and microquartz all within pore space in the radiolarian tests (Fig. 7C) suggests the mineralization stage I sulfides may have formed during the transformation of opaline silica to microquartz. The replacement of radiolaria is marked by sphalerite with a smooth core domain with few inclusions, potentially representing a pseudomorph of opaline silica. In contrast, inclusion-rich sphalerite is formed when it replaces the mudstone matrix (see Fig. 7C).

The biosiliceous nature of the host rock has resulted in some similarities in the style of mineralization-stage I sulfides of the Duo Lake Formation and the Niddery Lake Member, although there are also some key differences. The different gangue mineral assemblages within the two stratigraphic units correspond with key differences in protolith composition, particularly the presence of barite within the Niddery Lake Member. For example, barite replacement by Sp-$I_{stratabound}$ is associated with kaolinite and Ba-bearing mica formation (Fig. 8E, H). This assemblage may be linked to the release of Al that was incorporated into radiolaria tests or diagenetic transformation of preexisting illite and detrital muscovite (Friedman and Sanders, 1978; Steele et al., 2009). The formation of significant barian mica during mineralization stage I could have been controlled by the release of Ba during barite replacement.

In contrast, the Duo Lake Formation contains a lower abundance of phyllosilicate minerals (Fig. 11A). In samples where the phyllosilicates form >3% of the bulk mineralogy, most are concentrated within mm- to sub-mm-scale laminae that separate mineralized beds (Fig. 7B) and commonly comprise illite (Fig. 11B). These phases are also concentrated along stylolitic seams together with pyrobitumen (Fig. 7G), a typical outcome of pressure solution (e.g., Cox and Whitford-Stark, 1987) or thermal organic matter maturation (e.g., Schulz et al., 2016). The observed muscovite and minor illite in the mudstone are likely composed of detrital and premineralization phases. For example, detrital muscovite occurs as inclusions within Sp-$I_{stratabound}$ where the fluorapatite crystals coeval with the sphalerite cut across the mineral (Fig. 7F).

Timing of mineralization stage II

The second mineralization stage is the most volumetrically significant and is characterized by breccias and complex veins infilled by sphalerite, galena, pyrite, and minor chalcopyrite, all formed in four stages. The grade and intensity of mineralization stage II diminish outward from the breccia zones into the surrounding host rock mudstones of the Duo Lake and Portrait Lake Formations, where sulfides are confined to smaller, more locally developed veins and breccias (e.g., Fig. 9A).

The stockwork-style veins and breccias in mineralization stage II exhibit textures similar to the feeder zone mineralization described at the Tom and Jason deposits (Magnall et al., 2016a); however, in contrast to the Tom and Jason feeder zones, these are much more extensive, and clear crosscutting relationships between mineralization stage I and II exist (Fig. 7A), suggesting two genetically distinct stages of fluid flow. For example, stylolites are common in both the Duo Lake and Portrait Lake Formations at Boundary Zone, with some postdating mineralization stage I (Fig. 7G), whereas others appear to be cut across by veins hosting mineralization stage II sulfides (Fig. 9A inset).

The morphology of the fractures and breccias in the strata of both the Duo Lake and Portrait Lake Formations, including the angularity of remnant rock fragments and sharp contacts with the sulfides (Fig. 9G), is consistent with fluid-induced hydrothermal brecciation (Jébrak, 1997). This suggests that mineralization stage II may have formed simultaneously in these strata together with brecciation and vein formation or after the fracturing. For example, fluid overpressure could have led to fracture propagation along zones of weakness, such as preexisting fractures and stylolites (Martín-Martín et al., 2018).

The occurrence of significant pyrobitumen in the overmatured mudstones of the Duo Lake and Portrait Lake Formations, disseminated in matrix pores, stylolites, and minor veins (e.g., Fig. 7G), suggests that thermal cracking of liquid hydrocarbon has also occurred, which would also have contributed to increased pore pressures (Tian et al., 2008). This process can occur over a wide range of temperatures (<90° to ~250°C) and generate methane that could facilitate sulfate reduction in such units. Fracturing along stylolite seams would have provided a particularly effective mechanism for increasing permeability and enhancing the flow of metalliferous hydrothermal fluids. Indeed, some of the margins of the mineralized veins and breccias resemble stylolites (Fig. 9A inset), with insoluble residues comprising pyrobitumen, phyllosilicates, pyrite, and quartz (Fig. 5O). Importantly, the significant organic matter in the host rocks may have acted as a reductant, impacting the redox conditions during mineralization formation and resulting in the precipitation of sulfides and carbonate minerals such as siderite in reducing conditions.

In one Niddery Lake Member sample (Fig. 10E), the mineralization stage I assemblage is crosscut by mm- to cm-sized pyrite crystals that are coeval with fluorapatite, barite, and barian mica in a vein. The U-Pb geochronology of fluorapatite (Fig. 10E) predates both the Late Jurassic-Early Cretaceous folds and thrusts in the Macmillan Pass region (Abbott, 1982; McClay, 1991) and the Early-Middle Cretaceous metamorphism and granitoid emplacements (Gordey et al., 1991; Mair et al., 2006). The discordant veins clearly crosscut and postdate mineralization stage I; however, the precise relationship with mineralization stage II is unclear as an overlying fault precludes observation of this relationship.

The coarse-grained pyrite crystals in the vein are associated with coeval megaquartz pressure shadows, which are comparable to the low-grade metamorphic pyrite-quartz assemblage in matrix, veins, and quartz veins reported in the Macmillan Pass district (Ansdell et al., 1989). Leighton et

al. (2021) compared the subgreenschist facies metamorphic pyrite to similar occurrences in the Howard's Pass district, which are interpreted to have formed during the Cordilleran Mesozoic orogeny (Lianxing and McClay, 1992). During the Jurassic, exotic terranes were accreted onto the northern parts of the ancestral North America margin as part of the Cordilleran orogeny (Mair et al., 2006; Nelson and Colpron, 2007). If these veins formed as part of mineralization stage II, it would imply that this stage was coeval with Cordilleran deformation. However, the observation that high-angle stylolites (Fig. 5G) predate mineralization stage II would require either (1) an older, pre-Cordilleran phase of deformation, which is currently not documented in the area; or (2) that the high-angle stylolites formed during Cordilleran deformation, and that mineralization stage II formed syn- to post-Cordilleran deformation. The presence of barian mica in the dated vein and as part of the mineralization stage assemblage could indicate some components were recycled or that there was a separate influx of late-stage fluids enriched in these components.

In the Selwyn basin, Zn-Pb mineralization in various districts is largely interpreted to predate the Late Jurassic to Early Cretaceous deformation, with primary sedimentary and synmineralization features, as well as sulfides, believed to have been modified by deformation in both the Howard's Pass and Macmillan Pass districts (Gordey and Anderson, 1993; Gadd et al., 2015; Martel, 2017). Gadd et al. (2015) suggested that the tectonic overprint in the Howard's Pass district coincided with the formation of a porphyroblastic pyrite generation. This generation of pyrite overgrows earlier sulfides and is crystallographically aligned with the regional orogenic cleavage. Additionally, sulfides are suggested to have been remobilized and concentrated within pressure solution cleavage developed during the Cordilleran deformation (Martel, 2017). At the Macmillan Pass district, orogenic deformational features such as folding and faulting appear to have formed after the initial mineralization stage. However, some of these features have been interpreted as synsedimentary (Goodfellow, 2007; Leighton et al., 2019).

Development of phyllosilicate alteration: The phyllosilicate assemblages within the Boundary Zone rock types, comprising muscovite, kaolinite, and pyrophyllite, could reflect the influence of diagenetic, hydrothermal, and/or low-grade metamorphic processes that occurred during various stages of basin evolution. Pyrophyllite and kaolinite have been identified in barren and mineralized samples of volcaniclastic rocks, as well as interbedded mudstones, conglomerates, and diamictites within the Macmillan Pass Member (Fig. 11). This suggests a potential genetic link with both hydrothermal and background processes.

Kaolinite can form under early diagenetic (<100°C) to low anchizone conditions, and at higher temperatures (200°–300°C), this may be transformed to pyrophyllite (Merriman and Peacor, 1999). Notably, the transformation of kaolinite to pyrophyllite rather than illite is favored in aluminous, Fe-poor mudstones (Frey, 1987). Pyrophyllite is also observed in basins with extensive submarine volcanism coinciding with sedimentation (e.g., Merriman, 2006). Volcaniclastic material could be incorporated within the sediments and altered to pyrophyllite during burial diagenesis.

The presence of pyrophyllite in both barren and mineralized samples could also form part of a widespread alteration assemblage in the Macmillan Pass Member and volcaniclastic rocks. This interpretation is consistent with observations that pyrophyllite-quartz ± muscovite assemblages, which develop in volcaniclastics and related sedimentary rocks, can extend from the orebody into surrounding zones (e.g., Cox, 1981; Huston and Kamprad, 2001). In hydrothermal systems, the formation of pyrophyllite ± quartz ± muscovite assemblages typically occurs at temperatures ranging from 250° to over 300°C (Sverjensky et al., 1991; Huston and Kamprad, 2001; Will et al., 2016). However, in quartz-rich rock types similar to most of the sulfide host rocks at Boundary Zone (Fig. 11), pyrophyllite may have formed at slightly lower temperatures (e.g., Marumo, 1989).

Genesis of the Boundary Zone Zn-Pb ± Ag and implications for CD-type mineral systems

In the Macmillan Pass district, the CD-type Zn-Pb ± Ag mineralization at the Tom and Jason deposits is restricted to the Middle to Late Devonian Portrait Lake Formation (McClay, 1984; Goodfellow and Lydon, 2007). In this study, we describe a new deposit in the Macmillan Pass district where sulfide mineralization is in both the Middle to Late Devonian Portrait Lake Formation and Late Ordovician-Early Silurian Duo Lake Formation strata. Furthermore, we have documented that sulfide mineralization occurred in two distinct stages: a diagenetic stratabound host-rock replacement stage and a later, crosscutting breccia and vein-mineralization stage. Mineralization stage I involves the exploitation of primary pore space associated with radiolarian tests, whereas ore stage II primarily comprises brecciation of the host units.

Several studies have suggested subseafloor diagenetic replacement of host rock components as the main mechanism of stratiform and stratabound sulfide mineralization in CD-type deposits (Williams, 1978a, b; Kelley et al., 2004; Reynolds et al., 2021; Magnall et al., 2023). Magnall et al. (2015) suggested that the presence of highly biosiliceous Late Devonian mudstones at the Tom and Jason area facilitated porosity preservation and permeability pathways that were exploited by the mineralizing fluids during sediment burial. Our findings support this interpretation as we demonstrate that the diagenetic opaline silica transformation occurred at the same time as the precipitation of Sp-$I_{stratabound}$. During this transformation, a sphalerite-galena-pyrite-fluorapatite assemblage formed in the biosiliceous mudstones of the Duo Lake Formation, whereas sphalerite-galena-pyrite-barian mica ± chalcopyrite ± sulfosalts formed in the Niddery Lake Member of the Portrait Lake Formation. The lack of systematic variation in REE + Y + Sr + Mn contents of fluorapatite coeval with mineralization stage I sulfide from both strata (Fig. 10D) suggests a common fluid type. This supports the interpretation that the mineralization in both strata is the result of a similar event in different aged host rocks, occurring as a replacement in sediments undergoing burial diagenesis.

Biogenic silica can play a key role in the preservation of porosity in mudstones undergoing burial diagenesis (Milliken and Olson, 2017), with up to 60% porosity preservation down to hundreds of meters (Velde, 1996; Aplin and Macquaker,

2011; Milliken and Olson, 2017). Selective host-rock replacement (Hinman, 1995; Magnall et al., 2023) and pore filling (Milliken et al., 2016) are known to occur at depth during burial (Gao et al., 2022), and this supports the possibility of sulfide mineralization coupled with in situ opaline silica transformation in biosiliceous mudstones undergoing diagenesis. Nevertheless, it is surprising to find the same style of mineralization in units that would have been undergoing different stages of diagenesis, with the Duo Lake Formation at a greater depth. Based on true stratigraphic thickness measurements derived from 3-D geologic modeling that is supported by over 35,000 m of drilling, the top of mineralization stage I hosted in the Duo Lake Formation is known to be separated from the base of mineralization stage I in the Niddery Lake member by approximately 50 m of compacted sedimentary rock. Similarities in the selective host-rock replacement in either unit could either be explained by two separate stages of mineralization stage I fluid flow or by a delay in the opal-CT transition in the Duo Lake Formation, perhaps resulting from a greater component of aluminosilicate phases (Hinman, 1998).

Premineralization authigenic barite and byproducts of its dissolution (pyrite, celsian, barian mica) form a significant component of the mineralogy in the Niddery Lake Member. This is comparable to the Tom and Jason deposit host rocks, which also have thick packages of stratiform barite (McClay, 1984; Goodfellow et al., 1990; Magnall et al., 2016b). The stratiform barite at the Tom and Jason deposits suggests a common sulfur source during mineralization (Magnall et al., 2016b). We document petrographic evidence of overprinting premineralization barite, pyrite, and celsian, with barian mica forming part of the mineralization stage I assemblage at Boundary Zone. As such, tracing the Ba mass transfer associated with barite replacement into the gangue mineralogy will be important for understanding the lithogeochemical footprint of the mineralization.

With increasing burial diagenesis, progressive authigenic quartz cementation and organic matter maturation would have affected the mechanical properties of the host rocks, leading to fluid overpressure buildup and nontectonic fracturing (Tian et al., 2008; Milliken and Olson, 2017; Abu-Mahfouz et al., 2020). At Boundary Zone, fracturing, together with stylolitization, could have allowed for a subsequent fluid-induced brecciation driven by pore fluid pressure increase, thermal cracking, and, in part, metalliferous hydrothermal fluid inflow. The aqueous fluids for mineralization stage II high-grade Zn-Pb-Ag may have exploited these weaknesses, precipitating sphalerite, galena, pyrite, and associated chalcopyrite, siderite, and megaquartz that infilled and cemented fractures and breccias. The multiple sphalerite generations in the breccias and veins imply episodic and repeated inflow of mineralizing fluids during mineralization stage II formation. The timing of mineralization stage II is not well constrained. Comparable CD-type multistage systems have been described in the Red Dog district of the Kuna basin (Kelley et al., 2004; Slack et al., 2004b; Reynolds et al., 2015) and the George Fisher deposit in the Carpentaria Province (Chapman, 2004; Rieger et al., 2023).

Based on textural observations and coeval precipitation with sphalerite, the fluorapatite crystals are suggested to have a common origin with the mineralization-stage sulfides, which are hydrothermal in origin and precipitated at different periods during the two mineralization-forming stages. There is a general lack of systematic variation in the P_2O_5, CaO, and FeO contents (App. Table A1). Additionally, the lack of other Ca- and Na-bearing mineral phases in the mineralization stages and Na_2O content below the detection limit (138 µg/g) in all fluorapatite suggests they formed from F-rich and Ca- and Na-deficient fluids (Li and Zhou, 2015). Fluorapatite crystals have elevated Sr content and REE + Y + Sr + Mn contents. Sr^{2+} commonly substitutes for Ca^{2+} in apatite group minerals, whereas REEs are incorporated via coupled substitution reactions (Chakhmouradian et al., 2002; Pan and Fleet, 2002). Notably, although fluorapatite can form from F-poor hydrothermal fluids (Zhu and Sverjensky, 1991), the overlap observed in F and REE contents in both premineralization and mineralization stages suggests these elements were locally mobile and could largely be recycled (Milodowski and Zalasiewicz, 1991; Slack et al., 2004a); the mobility of the latter would be enhanced by the F-rich hydrothermal fluids (Haas et al., 1995; Huston, 2001).

In summary, petrographic, mineralogic, and geochronological data have allowed constraints to be placed on many aspects of the Boundary Zone mineralization system. Biogenic silica transformation coincided with hydrothermal fluid inflow, resulting in syndiagenetic stratabound mineralization that was later overprinted by breccia and vein sulfides of the second mineralization stage (Fig. 13). Understanding the relationships between mineralization and regional-scale biosiliceous mudstone deposition, barite formation, and nearby fault system dynamics will be essential for continued exploration in the Boundary Zone area.

Conclusions

The host rocks, tectonic setting, formation mechanisms, and observed petrographic and mineralogical features suggest the Boundary Zone Zn-Pb-Ag deposit is another CD-type system in the Macmillan Pass district, Yukon, Canada. The mineralization is characterized by early diagenetic stratabound replacement in biosiliceous mudstones of the Late Ordovician-Early Silurian Duo Lake Formation and Middle to Late Devonian Portrait Lake Formation, which is then overprinted by later breccia and vein mineralization. Syndiagenetic mineralization stage I stratabound sulfides formed mainly by replacing radiolarian tests during biogenic silica transformation in the mudstones. Barite replacement by sulfides adds to the significant mineralization stage I that is coeval with barian mica formation in the Niddery Lake Member. The dissolution-reprecipitation of quartz and barite dissolution generated permeability, which facilitated hydrothermal fluid flow. Mineralization stage II is primarily hosted in crosscutting veins and breccias in the Duo Lake and Portrait Lake Formations and comprises multiple generations of sulfides, siderite, and quartz, preserving evidence of repeated hydrothermal fluid flow in the fractures. The timing of sulfide formation in the two mineralization stages spans diagenetic periods of the host rocks that formed stratabound sulfides and vein- and breccia-hosted sulfides that may be related to regional deformational events. Phyllosilicate assemblages comprising muscovite, barian mica, kaolinite, and pyrophyllite indicate temperatures may have reached >240°C at Boundary Zone.

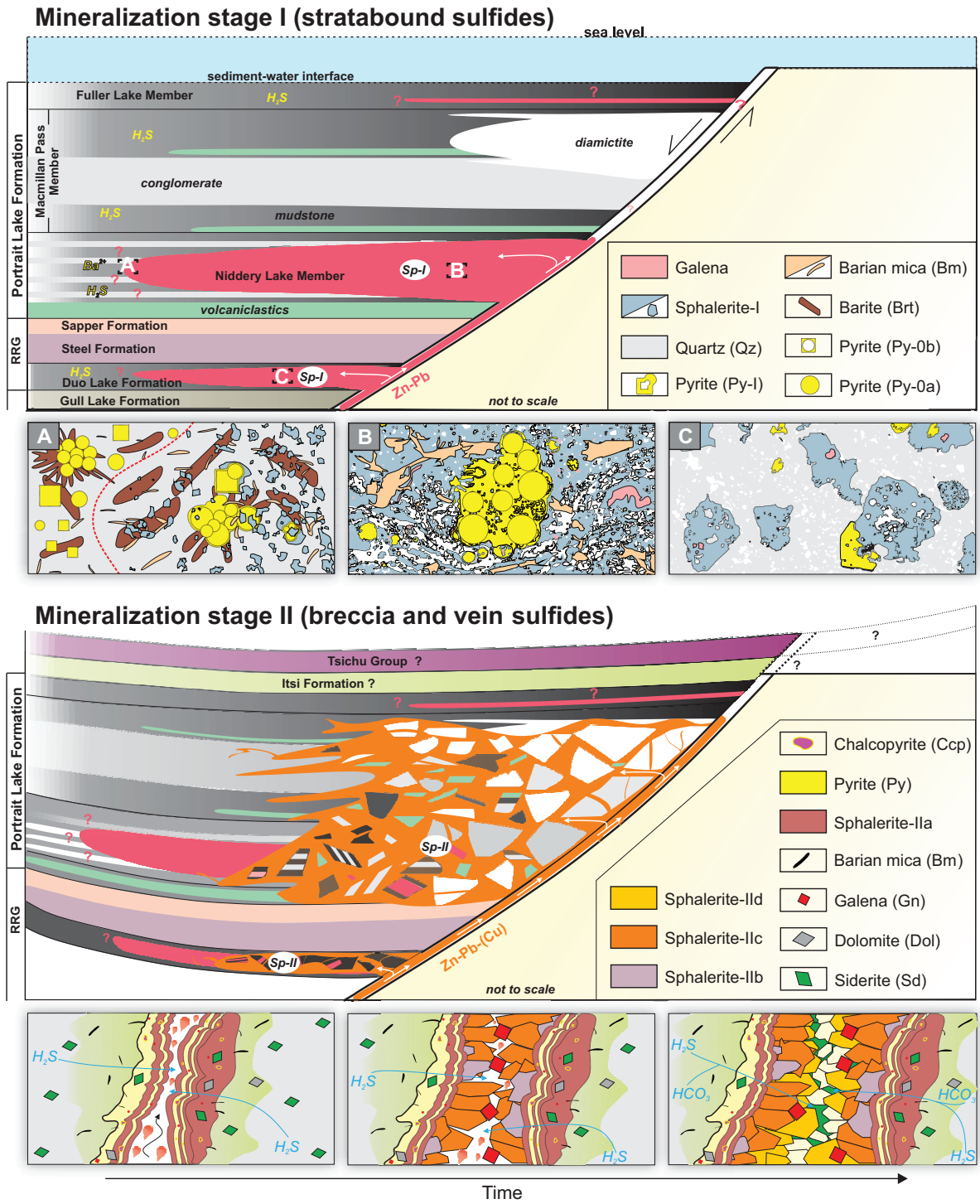

Fig. 13. Schematic diagrams of the two stages in the development of Zn-Pb mineralization at the Boundary Zone that are accompanied by silicification and sericite alteration in the wall rocks. During mineralization stage I, stratabound sulfides developed in the Duo Lake Formation and the Portrait Lake Formation. In all cases, premineralization Py-0 formed during early diagenesis through the interaction of H_2S with reactive Fe in the mudstones. The flow of metalliferous hydrothermal fluid interacted with the host rocks where Sp-$I_{stratabound}$, Gn-I, and Py-I form. Barian mica formed coeval with the sulfides in the Portrait Lake Formation. (B) The second mineralization period (mineralization stage II) is initiated when hydrothermal fluid with increased Cu^+ activity flows into veins and breccias, and Sp-$IIa_{colloform}$ precipitates together with Py-IIa and chalcopyrite with minor siderite and dolomite. The formation of coarse-grained Sp-$IIb_{metallic\text{-}brown}$ and Sp-$IIc_{sector\text{-}zoned}$ was accompanied by Gn-II that, together, formed the volumetrically major sulfide assemblage of Boundary Zone. The Sp-$IId_{pale\text{-}yellow}$ precipitated late, together with coarse-grained quartz and siderite. The thicknesses of the strata and inclinations are exaggerated and not to scale. Abbreviations: Bm = barian mica, Brt = barite, Ccp = chalcopyrite, Dol = dolomite, Gn = galena, Py = pyrite, Qz = quartz, RRG = Road River Group, Sd = siderite, Sp = sphalerite.

Acknowledgments

We are grateful for the Helmholtz-Rekrutierungsinitive to S. A. Gleeson, the Petroleum Technology Development Fund (PTDF), and the German Academic Exchange Service (DAAD) through cofinanced funding (Nr. 57473408). We also appreciate the financial support from the Society of Economic Geologists (SEG) 2022 Student Research Grant, Spora Explorers' Fund (Nr. SRG 22-19), to H. M. Grema. Fireweed Metals Corp. is deeply appreciated for access to their database and for providing samples for this study. We acknowledge technical support during data generation by Uwe Dittmann and Christine Fischer (thin sections and mounts preparation), Franziska H. Wilke (EPMA), Dilara Topal (clay-size XRD), Frédéric Couffignal (SIMS), and Michael Wiedenbeck for help with U-Pb data reduction. We thank our reviewers, David Huston and Steven Hollis, and Associate Editor Jonathan Cloutier, for their constructive feedback that significantly improved the quality of this manuscript.

REFERENCES

Abbott, J.G., 1982, Structure and stratigraphy of the Macmillan fold belt: Evidence for Devonian faulting, Yukon geology and exploration 1981: Whitehorse, Yukon, Department of Indian Affairs and Northern Development (Canada), Northern Affairs Program, Exploration and Geological Services Division, Open File 1983-1, p. 22–33.

——2013, Bedrock geology of the Macmillan Pass area Yukon and adjacent Northwest Territories (NTS 105O/1,2 and parts of 105O/7,8 and 105P/4,5): Yukon Geological Survey, Geoscience Map 2013-1.

Abbott, J.G., and Turner, R.J.W., 1991, Character and paleotectonic setting of Devonian stratiform sediment hosted Zn, Pb, Ba deposits, Macmillan fold belt, Yukon, *in* Abbott, J.G., and Turner, R.J.W., eds., Mineral deposits of the northern Canadian Cordillera, Yukon-Northeastern British Columbia [Field Trip 14]: Geological Survey of Canada, Open File 2169, p. 99–136, publications.gc.ca/site/eng/9.806646/publication.html.

Abbott, J.G., Gordey, S.P., and Tempelman-Kluit, D.J., 1986, Setting of stratiform, sediment-hosted lead-zinc deposits in Yukon and northeastern British Columbia: Canadian Institute of Mining and Metallurgy, Special Volume 37, p. 1–18, data.geology.gov.yk.ca/Reference/42332#InfoTab.

Abu-Mahfouz, I.S., Cartwright, J., Idiz, E., Hooker, J.N., and Robinson, S.A., 2020, Silica diagenesis promotes early primary hydrocarbon migration: Geology, v. 48, p. 483–487.

Ansdell, K.M., Nesbitt, B.E., and Longstaffe, F.J., 1989, A fluid inclusion and stable-isotope study of the Tom Ba-Pb-Zn deposit, Yukon Territory, Canada: Economic Geology, v. 84, p. 841–856.

Aplin, A.C., and Macquaker, J.H.S., 2011, Mudstone diversity: Origin and implications for source, seal, and reservoir properties in petroleum systems: American Association of Petroleum Geologists (AAPG) Bulletin, v. 95, p. 2031–2059.

Bailes, R.J., Smee, B.W., Blackader, D.W., and Gardner, H.D., 1986, Geology of the Jason lead-zinc-silver deposits, Macmillan Pass, eastern Yukon, *in* Morin, J.A., ed., Mineral deposits of northern Cordillera 37: The Canadian Institute of Mining and Metallurgy, p. 87–99.

Berner, R.A., Ruttenberg, K.C., Ingall, E.D., and Rao, J.-L., 1993, The nature of phosphorus burial in modern marine sediments, *in* Wollast, R., Mackenzie, F.T., and Chou, L., eds., Interactions of C, N, P and S biogeochemical cycles and global change, 4. NATO ASI Series: Springer Berlin Heidelberg, Springer, p. 365–378.

Blusson, S., 1978, Regional geological setting of lead-zinc deposits in Selwyn basin: Geological Survey of Canada, Yukon, Current Research, Part A, Paper 78-1A, p. 77–80.

Canet, C., Anadon, P., Gonzalez-Partida, E., Alfonso, P., Rajabi, A., Perez-Segura, E., and Alba-Aldave, L.A., 2014, Paleozoic bedded barite deposits from Sonora (NW Mexico): Evidence for a hydrocarbon seep environment of formation: Ore Geology Reviews, v. 56, p. 292–300.

Carne, R.C., 1979, Geological setting and stratiform lead-zinc-barite mineralization, Tom Claims, Macmillan Pass, Yukon Territory, Canada: Department of Indian and Northern Affairs, Open-File Report, 4. EGS 1979-4, 37 p.

Carne, R.C., and Cathro, R.J., 1982, Sedimentary-exhalative (Sedex) Zn-Pb-Ag deposits, northern Canadian Cordillera: Canadian Institute of Mining Bulletin, v. 75, p. 66–78.

Carter, S.C., Paytan, A., and Griffith, E.M., 2020, Toward an improved understanding of the marine barium cycle and the application of marine barite as a paleoproductivity proxy: Minerals, v. 10, article 421.

Cecile, M.P., 1982, The Lower Paleozoic Misty Creek embayment, Selwyn basin, Yukon and Northwest Territories: Geological Survey of Canada, Bulletin 335, p. 78.

——2000, Geology of the northeastern Niddery Lake map area, east-central Yukon and adjacent Northwest Territories: Geological Survey of Canada, 120 p.

Chakhmouradian, A.R., Reguir, E.P., and Mitchell, R.H., 2002, Strontium-apatite: New occurrences, and the extent of Sr-for-Ca substitution in apatite-group minerals: Canadian Mineralogist, v. 40, p. 121–136.

Chapman, L.H., 2004, Geology and mineralization styles of the George Fisher Zn-Pb-Ag deposit, Mount Isa, Australia: Economic Geology, v. 99, p. 233–255.

Cobbett, R.N., Colpron, M., Crowley, J.L., Cordey, F., Blodgett, R.B., and Orchard, M.J., 2020, Late Devonian magmatism and clastic deposition in the upper Earn Group (central Yukon, Canada) mark the transition from passive to active margin along western Laurentia: Canadian Journal of Earth Sciences, v. 58, p. 471–494.

Cox, M.A., and Whitford-Stark, J.L., 1987, Stylolites in the Caballos Novaculite, west Texas: Geology, v. 15, p. 439–442.

Cox, S.F., 1981, The stratigraphic and structural setting of the Mt. Lyell volcanic-hosted sulfide deposits: Economic Geology, v. 76, p. 231–245.

Doebelin, N., and Kleeberg, R., 2015, Profex: A graphical user interface for the Rietveld refinement program BGMN: Journal of Applied Crystallography, v. 48, p. 1573–1580.

Dumoulin, J.A., Harris, A.G., Blome, C.D., and Young, L.E., 2004, Depositional settings, correlation, and age of carboniferous rocks in the western Brooks Range, Alaska: Economic Geology, v. 99, p. 1355–1384.

Fernandes, N.A., Gleeson, S.A., Magnall, J.M., Creaser, R.A., Martel, E., Fischer, B.J., and Sharp, R., 2017, The origin of Late Devonian (Frasnian) stratiform and stratabound mudstone-hosted barite in the Selwyn basin, Northwest Territories, Canada: Marine and Petroleum Geology, v. 85, p. 1–15.

Fireweed Metal Corporation, 2021, Macmillan Pass: Growing a giant. Corporate presentation, 7th September 2021. https://fireweedmetals.com/fireweed-zinc-provides-final-boundary-zone-drill-results-and-a-2021-exploration-review/

Folk, R.L., and Pittman, J.S., 1971, Length-slow chalcedony; a new testament for vanished evaporites: Journal of Sedimentary Research, v. 41, p. 1045–1058.

Fraser, T.A., and Hutchison, M.P., 2017, Lithogeochemical characterization of the Middle-Upper Devonian Road River Group and Canol and Imperial formations on Trail River, east Richardson Mountains, Yukon: Age constraints and a depositional model for fine-grained strata in the Lower Paleozoic Richardson trough: Canadian Journal of Earth Sciences, v. 54, p. 731–765.

Fraser, T.A., Milton, J., and Gouwy, S.A, 2021, New geochemistry from old drill holes at the Tom property, Macmillan Pass, Yukon, in MacFarlane, K.E., ed., Yukon exploration and geology 2020: Yukon Geological Survey, p. 19–46.

Frey, M., 1987, The reaction-isograd kaolinite + quartz = pyrophyllite + H_2O, Helvetic Alps, Switzerland: Schweizerische Mineralogische und Petrographische Mitteilungen, v. 67, p. 1–11.

Friedman, G.M., and Sanders, J.E., 1978, Principles of sedimentology: New York, John Wiley and Sons, 792 p.

Gabrielse, H., 1967, Tectonic evolution of the northern Canadian Cordillera: Canadian Journal of Earth Sciences, v. 4, p. 271–298.

Gadd, M.G., Layton-Matthews, D., Peter, J.M., and Paradis, S.J., 2015, The world-class Howard's Pass SEDEX Zn-Pb district, Selwyn basin, Yukon. Part I: Trace element compositions of pyrite record input of hydrothermal, diagenetic, and metamorphic fluids to mineralization: Mineralium Deposita, v. 51, p. 319–342.

Gadd, M.G., Layton-Matthews, D., and Peter, J.M., 2016a, Non-hydrothermal origin of apatite in SEDEX mineralization and host rocks of the Howard's Pass district, Yukon, Canada: American Mineralogist, v. 101, p. 1061–1071.

Gadd, M.G., Layton-Matthews, D., Peter, J.M., and Paradis, S.J., 2016b, The world-class Howard's Pass SEDEX Zn-Pb district, Selwyn basin, Yukon. Part I: Trace element compositions of pyrite record input of hydrothermal,

diagenetic, and metamorphic fluids to mineralization: Mineralium Deposita, v. 51, p. 319–342.

Gadd, M.G., Layton-Matthews, D., Peter, J.M., Paradis, S., and Jonasson, I.R., 2017, The world-class Howard's Pass SEDEX Zn-Pb district, Selwyn basin, Yukon. Part II: The roles of thermochemical and bacterial sulfate reduction in metal fixation: Mineralium Deposita, v. 52, p. 405–419.

Gadd, M.G., Peter, J.M., Hnatyshin, D., Creaser, R., Gouwy, S., and Fraser, T., 2020, A Middle Devonian basin-scale precious metal enrichment event across northern Yukon (Canada): Geology, v. 48, p. 242–246.

Gao, P., Xiao, X.M., Hu, D.F., Lash, G.G., Liu, R.B., Cai, Y.D., Wang, Z.H., Zhang, B.Y., Yuan, T., and Liu, S.Y., 2022, Effect of silica diagenesis on porosity evolution of deep gas shale reservoir of the Lower Paleozoic Wufeng-Longmaxi formations, Sichuan basin: Marine and Petroleum Geology, v. 145, article 105873.

Gardner, H.D., and Hutcheon, I., 1985, Geochemistry, mineralogy, and geology of the Jason Pb-Zn deposits, Macmillan Pass, Yukon, Canada: Economic Geology, v. 80, p. 1257–1276.

Gonzalez-Muñoz, M., Martinez-Ruiz, F., Morcillo, F., Martin-Ramos, J., and Paytan, A., 2012, Precipitation of barite by marine bacteria: A possible mechanism for marine barite formation: Geology, v. 40, p. 675–678.

Goodfellow, W.D., 1987, Anoxic stratified oceans as a source of sulphur in sediment-hosted stratiform ZnPb deposits (Selwyn basin, Yukon, Canada): Chemical Geology: Isotope Geoscience Section, v. 65, p. 359–382.

——2004, Geology, genesis and exploration of SEDEX deposits, with emphasis on the Selwyn basin, Canada: New Delhi, Narosa Publishing House, 24–99 p.

——2007, Mineral deposits of Canada: A synthesis of major deposit-types, district metallogeny, the evolution of geological provinces, and exploration methods: Geological Association of Canada, Mineral Deposits Division, Special Publication no. 5, p. 1068.

Goodfellow, W.D., and Lydon, J.W., 2007, Sedimentary exhalative (SEDEX) deposits: Geological Association of Canada, Mineral Deposits Division, Special Publication no. 5, p. 163–183.

Goodfellow, W.D., Rhodes, D., Abbott, J., and Turner, R., 1990, Geological setting, geochemistry and origin of the Tom stratiform Zn-Pb-Ag-barite deposits, Mineral deposits of the northern Canadian Cordillera: International Association on the Genesis of Ore Deposits, Eighth Symposium, Ottawa, 1990, Field Trip 14, p. 177–244.

Goodfellow, W.D., Lydon, J.W., and Turner, R., 1993, Geology and genesis of stratiform sediment-hosted (SEDEX) zinc-lead-silver sulphide deposits, *in* Kirkham, R.V., Sinclair, W.D., Thorpe, R.I., and Duke, J.M., eds., Mineral deposit modeling: Geological Association of Canada, Special Paper 40, p. 201–251.

Goodfellow, W.D., Cecile, M.P., and Leybourne, M.I., 1995, Geochemistry, petrogenesis, and tectonic setting of lower Paleozoic alkalic and potassic volcanic rocks, northern Canadian Cordilleran miogeocline: Canadian Journal of Earth Sciences, v. 32, p. 1236–1254.

Gordey, S.P., and Anderson, R.G., 1993, Evolution of the northern Cordilleran miogeocline, Nahanni map area (105I), Yukon and Northwest Territories: Geological Survey of Canada, Memoir 428, 224 p.

Gordey, S.P., Geldsetzer, H.H.J., Morrow, D.W., Bamber, E.W., Henderson, C.M., Richards, B.C., McGugan, A., Gibson, D.W., and Poulton, T.P., 1991, Upper Devonian to Middle Jurassic assemblages, *in* Gabrielse, H., and Yorath, C. J., eds., Geology of the Cordilleran orogen in Canada: Geological Survey of Canada, 296 p.

Gordey, S.P., Macdonald, J.D., Turner, E.C., Long, D.G.F., Martel, E., and Fischer, B.J., 2010, Structural geology of the central Mackenzie Mountains, *in* Martel, E., Turner, E.C., and Fischer, B.J., eds., Geology of the central Mackenzie Mountains of the northern Canadian Cordillera, Sekwi Mountain (105P), Mount Eduni (106A), and northwestern Wrigley Lake (95M) map areas, Northwest Territories: Northwest Territories Geoscience Office, p. 215–250.

Grema, H.M., Magnall, J.M., Whitehouse, M.J., Gleeson, S.A., and Schulz, H.M., 2022, The formation of highly positive $\delta^{34}S$ values in Late Devonian mudstones: Microscale analysis of pyrite ($\delta^{34}S$) and barite ($\delta^{34}S$, $\delta^{18}O$) in the Canol Formation (Selwyn basin, Canada): Frontiers in Earth Science, v. 9, article 784824.

Grema, H.M., Wudarska, A., Wilke, F.D.H., Schleicher, A.M., Milton, J.E., Magnall, J.M., Gleeson, S.A., and Schulz, H.-M., 2024, Petrography, quantitative mineralogy, and U-Pb geochronology of the Boundary Zone Zn-Pb±Ag deposit, Yukon, Canada: GFZ Data Services, doi.org/10.5880/GFZ.3.1.2024.007.

Haas, J.R., Shock, E.L., and Sassani, D.C., 1995, Rare earth elements in hydrothermal systems: Estimates of standard partial molal thermodynamic properties of aqueous complexes of the rare earth elements at high pressures and temperatures: Geochimica et Cosmochimica Acta, v. 59, p. 4329–4350.

Hart, C.J.R., Goldfarb, R.J., Lewis, L.L., and Mair, J.L., 2004, The northern Cordilleran mid-Cretaceous plutonic province: Ilmenite/magnetite-series granitoids and intrusion-related mineralisation: Resource Geology, v. 54, p. 253–280.

Hayward, N., Magnall, J.M., Taylor, M., King, R., McMillan, N., and Gleeson, S.A., 2021, The Teena Zn-Pb deposit (McArthur basin, Australia). Part I: Syndiagenetic base metal sulfide mineralization related to dynamic subbasin evolution: Economic Geology, v. 116, p. 1743–1768.

Hinman, M., 1995, Base-metal mineralisation at McArthur River: Structure and kinematics of the HYC-Cooley zone at McArthur River: Australian Geological Survey Organisation Record, v. 5, 29 p.

Hinman, N.W., 1998, Sequences of silica phase transitions: Effects of Na, Mg, K, Al, and Fe ions: Marine Geology, v. 147, Is. 1, p. 13–24.

Huston, D.L., 2001, Geochemical dispersion about the Western Tharsis Cu-Au deposit, Mt Lyell, Tasmania: Journal of Geochemical Exploration, v. 72, p. 23–46.

Huston, D.L., and Kamprad, J., 2001, Zonation of alteration facies at western Tharsis: Implications for the genesis of Cu-Au deposits, Mount Lyell field, western Tasmania: Economic Geology, v. 96, p. 1123–1132.

Jébrak, M., 1997, Hydrothermal breccias in vein-type ore deposits: A review of mechanisms, morphology and size distribution: Ore Geology Reviews, v. 12, p. 111–134.

Jennings, D.S., and Jilson, G.A., 1986, Geology and sulfide deposits of Anvil Range, Yukon Territory, *in* Morin, J.A., ed., Mineral deposits of northern Cordillera: Canadian Institute of Mining and Metallurgy, Special Volume 37, p. 319–361.

Johnson, C.A., Slack, J.F., Dumoulin, J.A., Kelley, K.D., and Falck, H., 2018, Sulfur isotopes of host strata for Howards Pass (Yukon-Northwest Territories) Zn-Pb deposits implicate anaerobic oxidation of methane, not basin stagnation: Geology, v. 46, p. 619–622.

Jonasson, I.R., Goodfellow, W.D., and Morin, J.A., 1986, Sedimentary and diagenetic textures, and deformation structures within the sulphide zone of the Howards Pass (XY) Zn-Pb deposit, Yukon and Northwest Territories: Canadian Institute of Mining and Metallurgy, Special Volume 37, p. 51–70.

Jowitt, S.M., and McNulty, B.A., 2021, Battery and energy metals: Future drivers of the minerals industry?: SEG Discovery, no. 127, p. 11–18.

Kabanov, P., 2019, Devonian (c. 388–375 Ma) Horn River Group of Mackenzie Platform (NW Canada) is an open-shelf succession recording oceanic anoxic events: Journal of the Geological Society, v. 176, p. 29–45.

Kelley, K.D., Leach, D.L., Johnson, C.A., Clark, J.L., Fayek, M., Slack, J.F., Anderson, V.M., Ayuso, R. A., and Ridley, W.I., 2004, Textural, compositional, and sulfur isotope variations of sulfide minerals in the Red Dog Zn-Pb-Ag deposits, Brooks Range, Alaska: Implications for ore formation: Economic Geology, v. 99, p. 1509–1532.

Kirkham, G., Dunning, J., and Schleiss, W., 2012, Update for Don deposit mineral resource estimate, Howard's Pass property, eastern Yukon: NI 43-101 technical report for Selwyn Resources Ltd., 145 p.

Landry, P., Hamilton, C., and McLeod, K.S., 2024, Technical report for NI 43-101 for the Macpass Project, Yukon, Canada: SLR Consulting (Canada) Ltd., SLR Project No. 205.030126.00001, sedarplus.ca/csa-party/records/document.html?id=0e6c5e13ce0a42b51472be7ad0e82577c9c7f49829bca85de02a68b5e2e0f0eb.

Leach, D.L., Sangster, D.F., Kelley, K.D., Large, R.R., Garven, G., Allen, C.R., Gutzmer, J., and Walters, S., 2005, Sediment-hosted lead-zinc deposits: A global perspective: Economic Geology, 100th Anniversary Volume, p. 561–608.

Leighton, C., Layton-Matthews, D., Peter, J.M., and Gadd, M., 2019, Application of pyrite chemistry to recognize a distal expression of hydrothermal activity in the MacMillan Pass SEDEX district, Yukon: Geological Survey of Canada, Open File 8549, p. 125–137.

Leighton, C., Layton-Matthews, D., Peter, J.M., Gadd, M.G., Voinot, A., and Leybourne, M.I., 2021, Paleoredox conditions, hydrothermal history, and target vectoring in the Macmillan Pass base-metal district, Yukon, Canada: 2-pyrite paragenesis and mineral chemistry: Canadian Mineralogist, v. 59, p. 1233–1259.

Li, X.C., and Zhou, M.F., 2015, Multiple stages of hydrothermal REE remobilization recorded in fluorapatite in the Paleoproterozoic Yinachang Fe-Cu-(REE) deposit, southwest China: Geochimica et Cosmochimica Acta, v. 166, p. 53–73.

Lianxing, G., and McClay, K.R., 1992, Pyrite deformation in stratiform lead-zinc deposits of the Canadian Cordillera: Mineralium Deposita, v. 27, p. 169–181.

Ludwig, K.R., 2012, User's manual for Isoplot 3.75: A geochronological toolkit for Microsoft Excel: Berkeley Geochronology Center, Special Publication no. 5, 75 p.

Magnall, J.M., Gleeson, S.A., and Paradis, S., 2015, The importance of siliceous radiolarian-bearing mudstones in the formation of sediment-hosted Zn-Pb ± Ba mineralization in the Selwyn basin, Yukon, Canada: Economic Geology, v. 110, p. 2139–2146.

Magnall, J.M., Gleeson, S.A., Blamey, N.J.F., Paradis, S., and Luo, Y., 2016a, The thermal and chemical evolution of hydrothermal vent fluids in shale hosted massive sulphide (SHMS) systems from the MacMillan Pass district (Yukon, Canada): Geochimica et Cosmochimica Acta, v. 193, p. 251–273.

Magnall, J.M., Gleeson, S.A., Stern, R.A., Newton, R.J., Poulton, S.W., and Paradis, S., 2016b, Open system sulphate reduction in a diagenetic environment—isotopic analysis of barite ($\delta^{34}S$ and $\delta^{18}O$) and pyrite ($\delta^{34}S$) from the Tom and Jason Late Devonian Zn-Pb-Ba deposits, Selwyn basin, Canada: Geochimica et Cosmochimica Acta, v. 180, p. 146–163.

Magnall, J.M., Gleeson, S.A., and Paradis, S., 2020, A new subseafloor replacement model for the Macmillan Pass clastic-dominant Zn-Pb ± Ba deposits (Yukon, Canada): Economic Geology, v. 115, p. 953–959.

Magnall, J.M., Wirth, R., Hayward, N., Gleeson, S.A., and Schreiber, A., 2023, Stratiform host-rock replacement via self-sustaining reactions in a clastic-dominated (CD-type) Zn deposit: Economic Geology, v. 118, p. 823–836.

Mair, J.L., Hart, C.J.R., and Stephens, J.R., 2006, Deformation history of the northwestern Selwyn basin, Yukon, Canada: Implications for orogen evolution and mid-Cretaceous magmatism: Geological Society of America Bulletin, v. 118, p. 304–323.

Martel, E., 2017, The importance of structural mapping in ore deposits—a new perspective on the Howard's Pass Zn-Pb district, Northwest Territories, Canada: Economic Geology, v. 112, p. 1285–1304.

Martel, E., Turner, E.C., and Fischer, B.J., 2011, Geology of the central Mackenzie Mountains of the northern Canadian Cordillera: Sekwi Mountain (105P), Mount Eduni (106A), and northwestern Wrigley Lake (95M) map areas, Northwest Territories: Northwest Territories (NWT) Geoscience Office, 423 p.

Martín-Martín, J., Gomez-Rivas, E., Gómez-Gras, D., Travé, A., Ameneiro, R., Koehn, D., and Bons, P., 2018, Activation of stylolites as conduits for overpressured fluid flow in dolomitized platform carbonates: Geological Society, London, Special Publication no. 459, p. 157–176.

Marumo, K., 1989, Genesis of kaolin minerals and pyrophyllite in Kuroko deposits of Japan: Implications for the origins of the hydrothermal fluids from mineralogical and stable isotope data: Geochimica et Cosmochimica Acta, v. 53, p. 2915–2924.

McClay, K.R., 1984, The geology of the Tom deposit, MacMillan Pass, Yukon Territory, Canada: Geological Association of Canada, Short Course Notes, v. 2, pt. 2, p. 60–96.

——1991, Deformation of stratiform Zn-Pb (-barite) deposits in the northern Canadian Cordillera: Ore Geology Reviews, v. 6, p. 435–462.

Merriman, R.J., 2006, Clay mineral assemblages in British Lower Palaeozoic mudrocks: Clay Minerals, v. 41, p. 473–512.

Merriman, R.J., and Peacor, D.R., 1999, Very low-grade metapelites: mineralogy, microfabrics and measuring reaction progress, *in* Frey, M., and Robinson, D., eds., Low-grade metamorphism: Oxford, Blackwell Science Ltd., p. 10–60.

Milliken, K.L., and Olson, T., 2017, Silica diagenesis, porosity evolution, and mechanical behavior in siliceous mudstones, Mowry shale (Cretaceous), Rocky Mountains, U.S.A: Journal of Sedimentary Research, v. 87, p. 366–387.

Milliken, K.L., Ergene, S.M., and Ozkan, A., 2016, Quartz types, authigenic and detrital, in the Upper Cretaceous Eagle Ford Formation, South Texas, USA: Sedimentary Geology, v. 339, p. 273–288.

Milodowski, A.E., and Zalasiewicz, J.A., 1991, Redistribution of rare earth elements during diagenesis of turbidite/hemipelagite mudrock sequences of Llandovery age from central Wales: Geological Society of London, Special Publication no. 57, p. 101–124.

Milton, J.E., Hickey, K.A., Gleeson, S.A., and Friedman, R.M., 2017, New U-Pb constraints on the age of the Little Dal basalts and Gunbarrel-related volcanism in Rodinia: Precambrian Research, v. 296, p. 168–180.

Monger, J.W.H., Price, R.A., and Tempelman-Kluit, D.J., 1982, Tectonic accretion and the origin of the two major metamorphic and plutonic welts in the Canadian Cordillera: Geology, v. 10, p. 70–75.

Morganti, J.M., 1979, The geology and ore deposits of the Howards Pass area, Yukon and Northwest Territories: The origin of basinal sedimentary stratiform sulphides deposits: Unpub. Ph.D. thesis, Vancouver, University of British Columbia, 351 p., open.library.ubc.ca/cIRcle/collections/ubctheses/831/items/1.0052838.

——1981, Ore deposit models—4. Sedimentary-type stratiform ore deposits: Some models and a new classification: Geoscience Canada, v. 8, p. 65–75.

Nelson, J., and Colpron, M., 2007, Tectonics and metallogeny of the British Columbia, Yukon and Alaskan Cordillera, 1.8 Ga to the present: Geological Association of Canada, Mineral Deposits Division, Special Publication no. 5, p. 755–791.

Ootes, L., Gleeson, S.A., Turner, E., Rasmussen, K., Gordey, S., Falck, H., Martel, E., and Pierce, K., 2013, Metallogenic evolution of the Mackenzie and eastern Selwyn Mountains of Canada's Northern Cordillera, Northwest Territories: A compilation and review: Geoscience Canada, v. 40, p. 40–69.

Pan, Y.M., and Fleet, M.E., 2002, Compositions of the apatite-group minerals: Substitution mechanisms and controlling factors: Phosphates: Geochemical, Geobiological, and Materials Importance, v. 48, p. 13–49.

Paytan, A., Mearon, S., Cobb, K.M., and Kastner, M., 2002, Origin of marine barite deposits: Sr and S isotope characterization: Geology, v. 30, p. 747–750.

Piccoli, P.M., and Candela, P.A., 2002, Apatite in igneous systems: Phosphates: Geochemical, Geobiological, and Materials Importance, v. 48, p. 255–292.

Pigage, L.C., 1991, Field guide Anvil Pb-Zn-Ag district, Yukon Territory, Canada: Geological Survey of Canada, Open File 2169, p. 177–244.

Potter, P.E., Maynard, J.B., and Depetris, P.J., 2005, Mud and mudstones: Introduction and overview: Berlin Heidelberg, Springer, 297 p.

Rajabi, A., Canet, C., Rastad, E., and Alfonso, P., 2015, Basin evolution and stratigraphic correlation of sedimentary-exhalative Zn-Pb deposits of the Early Cambrian Zarigan-Chahmir basin, Central Iran: Ore Geology Reviews, v. 64, p. 328–353.

Reynolds, M.A., Gingras, M.K., Gleeson, S.A., and Stemler, J.U., 2015, More than a trace of oxygen: Ichnological constraints on the formation of the giant Zn-Pb-Ag ± Ba deposits, Red Dog district, Alaska: Geology, v. 43, p. 867–870.

Reynolds, M.A., Gleeson, S.A., Creaser, R.A., Friedlander, B.A., Haywood, J.C., Hnatyshin, D., McCusker, J., and Waldron, J.W.F., 2021, Diagenetic controls on the formation of the Anarraaq clastic-dominated Zn-Pb-Ag deposit, Red Dog district, Alaska: Economic Geology, v. 116, p. 1803–1824.

Rieger, P., Magnall, J.M., Gleeson, S.A., and Oelze, M., 2023, Pyrite chemistry records a multistage ore forming system at the Proterozoic George Fisher massive sulfide Zn-Pb-Ag deposit, Mount Isa, Australia: Frontiers in Earth Science, v. 11, article 892759.

Salama, W., Khirekesh, Z., Amini, A., and Bafti, B.S., 2018, Diagenetic evolution of the upper Devonian phosphorites, Alborz for Mountain Range, northern Iran: Sedimentary Geology, v. 376, p. 90–112.

Sangster, D.F., 2002, The role of dense brines in the formation of vent-distal sedimentary-exhalative (SEDEX) lead-zinc deposits: Field and laboratory evidence: Mineralium Deposita, v. 37, p. 149–157.

Scanlan, E., 2022, A geochemical study of Paleozoic alkaline magmatism in the Selwyn basin and the potential relationship to Zn-Pb mineralization: Unpub. Ph.D. thesis, Kingston, Ontario, Canada, Queen's University, 249 p.

Schulz, H.M., Wirth, R., and Schreiber, A., 2016, Organic-inorganic rock-fluid interactions in stylolitic micro-environments of carbonate rocks: A FIB-TEM study combined with a hydrogeochemical modelling approach: Geofluids, v. 16, p. 909–924.

Slack, J.F., Dumoulin, J.A., Schmidt, J.M., Young, L.E., and Rombach, C.S., 2004a, Paleozoic sedimentary rocks in the Red Dog Zn-Pb-Ag district and vicinity, western Brooks Range, Alaska: Provenance, deposition, and metallogenic significance: Economic Geology, v. 99, p. 1385–1414.

Slack, J.F., Kelley, K.D., Anderson, V.M., Clark, J.L., and Ayuso, R.A., 2004b, Multistage hydrothermal silicification mad Fe-Tl-As-Sb-Ge-REE enrichment in the Red Dog Zn-Pb-Ag district, northern Alaska: Geochemistry, origin, and exploration applications: Economic Geology, v. 99, p. 1481–1508.

Slack, J.F., Falck, H., Kelley, K.D., and Xue, G.G., 2017, Geochemistry of host rocks in the Howards Pass district, Yukon-Northwest Territories, Canada: Implications for sedimentary environments of Zn-Pb and phosphate mineralization: Mineralium Deposita, v. 52, p. 565–593.

Steele, J.H., Thorpe, S.A., and Turekian, K.K., 2009, Marine chemistry and geochemistry: USA, Academic Press, 656 p.

Sverjensky, D.A., Hemley, J.J., and D'Angelo, W.M., 1991, Thermodynamic assessment of hydrothermal alkali feldspar-mica-aluminosilicate equilibria: Geochimica et Cosmochimica Acta, v. 55, p. 989–1004.

Tian, H., Xiao, X.M., Wilkins, R.W.T., and Tang, Y.C., 2008, New insights into the volume and pressure changes during the thermal cracking of oil to gas in reservoirs: Implications for the in-situ accumulation of gas cracked from

oils: American Association of Petroleum Geologists (AAPG) Bulletin, v. 92, p. 181–200.
Torres, M.E., Bohrmann, G., Dubé, T.E., and Poole, F.G., 2003, Formation of modern and Paleozoic stratiform barite at cold methane seeps on continental margins: Geology, v. 31, p. 897–900.
Turner, R.J.W., 1986, The genesis of stratiform lead-zinc deposits, Jason property, Macmillan Pass, Yukon: Ph.D. thesis, Stanford, Connecticut, Stanford University, 205 p., emrlibrary.gov.yk.ca/theses/turner_r_1986.pdf.
Turner, R.J.W., and Rhodes, D., 1990, Boundary Creek zinc deposit (Nidd property), MacMillan Pass, Yukon: Subseafloor sediment-hosted mineralization associated with volcanism along a Late Devonian syndepositional fault: Geological Survey of Canada, Paper 90, p. 321–335.
Valckx, N., Stuermer, M., Seneviratne, D., and Prasad, A., 2021, Metals demand from energy transition may top current global supply: IMF-Blog, 8 December 2021, www.imf.org/en/Blogs/Articles/2021/12/08/metals-demand-from-energy-transition-may-top-current-global-supply.
Velde, B., 1996, Compaction trends of clay-rich deep sea sediments: Marine Geology, v. 133, p. 193–201.
Weller, R.M., and Behl, R.J., 2017, Defining mechanical and compositional heterogeneity of highly siliceous mudstones: Upper Monterey Formation, Belridge oil field, San Joaquin basin, California: American Association of Petroleum Geologists, Search and Discovery, article 51432, www.searchanddiscovery.com/pdfz/documents/2017/51431weller/ndx_weller.pdf.html.
Will, P., Lüders, V., Wemmer, K., and Gilg, H.A., 2016, Pyrophyllite formation in the thermal aureole of a hydrothermal system in the Lower Saxony basin, Germany: Geofluids, v. 16, p. 349–363.
Williams, N., 1978a, Studies of the base metal sulfide deposits at McArthur River, Northern Territory, Australia; I, the Cooley and Ridge deposits: Economic Geology, v. 73, p. 1005–1035.
——1978b, Studies of the base metal sulfide deposits at McArthur River, Northern Territory, Australia; II, the sulfide-S and organic-C relationships of the concordant deposits and their significance: Economic Geology, v. 73, p. 1036–1056.
Wu, F.Y., Mitchell, R.H., Li, Q.L., Zhang, C., and Yang, Y.H., 2017, Emplacement age and isotopic composition of the Prairie Lake carbonatite complex, Northwestern Ontario, Canada: Geological Magazine, v. 154, p. 217–236.
Zhu, C., and Sverjensky, D.A., 1991, Partitioning of F-Cl-OH between minerals and hydrothermal fluids: Geochimica et Cosmochimica Acta, v. 55, p. 1837–1858.

Haruna Grema is a doctoral researcher at the GFZ Helmholtz Centre in Potsdam and at Freie Universität Berlin, Germany. He earned his B.Sc. in geology and M.Sc. in mineral exploration from Ahmadu Bello University, Zaria, Nigeria, where he conducted research on the provenance of alluvial gold within the metasedimentary belt of northwestern Nigeria. His current doctoral research is focused on the development of metal traps and the formation mechanisms of sediment-hosted Zn-Pb ± Ag deposits in the Macmillan Pass district, Yukon, Canada. Haruna utilizes a combination of multiscale petrography, mineralogical, microthermometric, and geochemical analyses in his research.